RTO WG 10: Test Cases for CFD Validation of Hypersonic Flight

Doyle Knight*

Dept of Mechanical and Aerospace Engineering

Rutgers - The State University of New Jersey

98 Brett Road, Piscataway, NJ 08854-8058

The NATO Research Technology Organization (RTO) Advanced Vehicle Technology (AVT) Panel established Working Group 10 (WG 10) "Technologies for Propelled Hypersonic flight" in 1998. The Terms of Reference included three Subgroups: 1) aerospike plug nozzle, 2) RAM/SCRAM jet configurations, and 3) Computational Fluid Dynamics (CFD) validation. An overview of Subgroup 3 (SG 3) is presented in this paper. The SG 3 participants defined six topical areas for which validation of CFD methodologies was deemed essential for effective analysis and design of propelled hypersonic vehicles. The topics are boundary layer instability and transition, real gas flows, laminar hypersonic viscous-inviscid interactions, shock-shock interactions, shock wave-turbulent boundary layer interaction, and base flows with and without plume interaction. A set of experiments were selected by Subgroup 3 participants for each topic and computations were solicited. The experiments are described in this paper. The results of the computations are presented in separate papers.

Introduction

The objective of this paper is to document a set of experiments for validation of CFD capability for specific flow phenomena relevant to hypersonic flight. The topic areas were established by NATO RTO Working Group 10 Subgroup 3 at its first meeting in December 1998 in Chalais-Meudon, France, and finalized at its meetings in June 1999 in Norfolk, Virginia, and November 1999 in Lampoldshausen, Germany. The topic areas and team leaders are listed in Table 1. In each area, specific experiments were selected by the Subgroup for CFD validation. The team leaders for each topic prepared the sections in this paper and solicited participants to contribute one or more computations. A website is available at: http://www.engr.rutgers.edu/~wg10.

The following sections contain a description of the selected experiments. In some cases, nominal freestream test conditions are provided and do not necessarily represent the exact freestream test conditions for which experimental data was obtained. The individual researchers should be contacted in all cases for the exact freestream test conditions.

A summary of the computations for each of the topic areas are presented in a series of AIAA papers at the AIAA 39th and 40th Aerospace Sciences Meetings. The list of papers is shown in Table 2.

A selected set of computations are described in detail in a series of papers at the AIAA 40th Aerospace Sciences Meeting. The list of papers is shown in Table 3.

---

*Professor, Dept of Mechanical and Aerospace Engineering; Associate Fellow, AIAA. Chairperson, RTO WG 10 SG 3.

1. BOUNDARY LAYER INSTABILITY AND TRANSITION
TEAM LEADER: S. SCHNEIDER

Prepared by

S. Schneider

General Introduction

Laminar-turbulent transition has a significant influence on hypersonic heat transfer, boundary-layer separation, and drag. Transition is affected by many factors, including freestream noise, roughness, waviness, geometry, Mach number, and wall temperature. Possible mechanisms include the first and second-mode instabilities, the 3D crossflow instability, the concave-wall Görtler instability, and streamwise vorticity. Saric *et al*[1] present a recent review. Experimental data that measures only transition location is difficult to analyze since the mechanism is often completely unknown; the systematic uncertainty cannot in general be resolved. Correlations of transition which ignore the transition mechanisms can only be valid for the conditions of the pre-existing correlated data. Attempts to correlate a wide range of transition data using algebraic formulas suffer from scatter that spans an order of magnitude (see Schneider[2]).

Reliable predictive methods will have to be based on simulations of the transition mechanisms. The best developed of these mechanism-based methods is the e^N method, which compares the integrated growth of the dominant instability waves to empirical transition data. More advanced mechanism-based methods include Direct Numerical Simulations or use of the Parabolized Stability Equations. A necessary step in the further development of these methods is accurate

1. REPORT DATE	2. REPORT TYPE	3. DATES COVERED
01 JAN 2006	**N/A**	**-**

4. TITLE AND SUBTITLE	5a. CONTRACT NUMBER
RTO WG 10: Test Cases for CFD Validation of Hypersonic Flight	5b. GRANT NUMBER
	5c. PROGRAM ELEMENT NUMBER
6. AUTHOR(S)	5d. PROJECT NUMBER
	5e. TASK NUMBER
	5f. WORK UNIT NUMBER

7. PERFORMING ORGANIZATION NAME(S) AND ADDRESS(ES)	8. PERFORMING ORGANIZATION REPORT NUMBER
Department of Mechanical and Aerospace Engineering Rutgers-The State University of New Jersey 98 Brett Road Piscataway, NJ 08854-8058	

9. SPONSORING/MONITORING AGENCY NAME(S) AND ADDRESS(ES)	10. SPONSOR/MONITOR'S ACRONYM(S)
	11. SPONSOR/MONITOR'S REPORT NUMBER(S)

12. DISTRIBUTION/AVAILABILITY STATEMENT
Approved for public release, distribution unlimited

13. SUPPLEMENTARY NOTES
See also ADM001860, Technologies for Propelled Hypersonic Flight (Technologies des vols hypersoniques propulses)., The original document contains color images.

14. ABSTRACT

15. SUBJECT TERMS

16. SECURITY CLASSIFICATION OF:			17. LIMITATION OF ABSTRACT	18. NUMBER OF PAGES	19a. NAME OF RESPONSIBLE PERSON
a. REPORT **unclassified**	b. ABSTRACT **unclassified**	c. THIS PAGE **unclassified**	**UU**	**24**	

Table 1   Topics and Team Leaders

Topic	Title	Team Leader(s)
1	Boundary Layer Instability and Transition	Steven Schneider (Purdue Universty)
2	Real Gas Flows	Graham Candler (University of Minnesota)
3	Laminar Viscous-Inviscid Interactions	Michael Holden (CUBRC)
4	Shock-Shock Interactions	Steven Walker and John Schmisseur (AFOSR)
5	Shock Wave-Turbulent Boundary Layer Interactions	Doyle Knight (Rutgers University)
6	Base Flows with and without Plume Interactions	Peter Bakker(Technical University of Delft)
		Phillipe Reijasse (ONERA)

Table 2   Topics and Papers

Topic	Author(s)	Title	Paper No.
OV	Jean Muylaert	RTO Working Group 10: Technologies for Propelled Hypersonic Flight	AIAA 2002-0432
1	Steven Schneider	Hypersonic Laminar Instability on Round Cones Near Zero Angle of Attack	AIAA 2001-0206
2	Graham Candler	CFD Validation for Hypersonic Flight: Real Gas Flows	AIAA 2002-0434
3	Michael Holden and Timothy Wadhams	Code Validation Study of Laminar Shock/Boundary Layer and Shock/Shock Interactions in Hypersonic Flow Part A: Experimental Measurements	AIAA 2001-1031*
3	John Harvey, Michael Holden and Timothy Wadhams	Code Validation Study of Laminar Shock/Boundary Layer and Shock/Shock Interactions in Hypersonic Flow Part B: Comparison with Navier-Stokes and DSMC Solutions	AIAA 2001-1031*
3	Michael Holden and John Harvey	Comparisons Between DSMC and Navier-Stokes Solutions on Measurements in Regions of Laminar Shock Wave Boundary Layer Interaction in Hypersonic Flow	AIAA 2002-0435
4	Steven Walker and John Schmisseur	CFD Validation of Shock Shock Interaction Flowfields	AIAA 2002-0436
5	Doyle Knight, Hong Yan, Argyris Panaras and Alexander Zheltovodov	RTO WG 10: CFD Validation for Shock Wave Turbulent Boundary Layer Interactions	AIAA 2002-0437
6	Peter Bakker, Willem Bannink and Phillipe Reijasse	Base Flows With and Without Plume Interactions	AIAA 2002-0438

OV   Overview of RTO Working Group 10
*There are two papers

Table 3   Topics and Papers

Topic	Author(s)	Title	Paper No.
2	Graham Candler, I. Nompelis, M. C. Druguet, I. Boyd and W.-L. Wang	CFD Validation for Hypersonic Flight Hypersonic Double-Cone Flow Simulations	AIAA 2002-0581
4	Dominic D'Ambrosio	Numerical Prediction of Shock / Shock Interactions in Hypersonic Flow	AIAA 2002-0582
5	Frederic Thivet	Lessons Learned From RANS Simulations of 3D Shock Wave Boundary Layer Interactions	AIAA 2002-0583

computation of the actual instability-wave growth, which is not trivial. For hypersonic flight vehicles with reasonably smooth walls, transition is likely to occur via the growth of linear-instability waves, so methods such as e^N are an appropriate approach to prediction.

Most ground-test data are contaminated by the high levels of noise which normally radiate from the turbulent boundary layers on the nozzle walls.[3] Even in these noisy conventional tunnels, there are few measurements of the instability mechanisms causing transition. Of these instability measurements, few have been carried out with calibrated instruments and well-documented conditions, so that a fairly reliable comparison to computations can be carried out.

The team feels that the following elements should be present in code-validation experiments for hypersonic transition:

- Detailed and reliable measurements of the transition mechanisms

- Accurate knowledge of the mean flow

  This includes repeated checks of boundary layer symmetry, instrumentation calibrations, tunnel flow nonuniformity effects, repeatability, etc. Moreover, close agreement between computation and experiment for mean flow characteristics is essential. This requires repeated tunnel entries and cooperation between experiments and computations.

- Accurate measurements of the fluctuating flow-field

  Comparison with linear instability theory requires calibrated measurements of the fluctuations at a known position in the eigenfunction. It seems possible that these might be carried out in conventional tunnels using ensemble averaging of controlled disturbances.

- Experiments in quiet tunnels

  Nonlinear secondary breakdown effects are dependent on small fluctuations combining with the primary instability. It seems doubtful that these can be repeatably and successfully studied except in quiet tunnels, since even controlled secondary disturbances may be swamped by tunnel noise. For similar reasons, receptivity experiments may also require quiet flow.

These specifications are updated from Reshotko.[4] This earlier reference gives additional suggestions, and shows the long-term importance of a coordinated approach. Unfortunately, these specifications are extremely difficult to meet at hypersonic speeds. Although new experimental efforts are underway at Purdue and at the Institute of Theoretical and Applied Mechanics (ITAM), Novosibirsk, Russia, all existing data fall short.

Three experimental datasets are described below. A detailed analysis of the datasets and prior computations is presented in Schneider.[5] While all three datasets contain significant flaws and limitations, they are the best presently available, in the opinion of the team. Accurate computation of the wave growth and eigenfunctions for these cases would be a significant step towards the further development of mechanism-based methods. Comparisons between the experiments and the results of multiple independent computations would shed light on the strong and weak elements in all, and aid in the development of new work.

Because of the limited resources presently available, attention is focused on axisymmetric geometries. The computational resources required are much less than in the 3D case. All of the datasets are for cold hypersonic flow without chemistry, because detailed measurements of the mechanisms of hot hypersonic transition do not exist. Although the data shown below are primarily measurements of the cold-flow second-mode instability, other mechanisms do of course remain important (e.g., Hornung[6]).

Dataset No. 1: Sharp Cone at Mach 8

Prepared by

S. Schneider

Introduction

Stetson *et al*[7,8] carried out calibrated measurements of instability wave growth on several conical models in AEDC Tunnel B at Mach 8, during the late 1970's and early 1980's. Detailed hot-wire measurements were carried out in this expensive production tunnel by J. Donaldson, under the direction of K. Stetson. The experiments focused on the hypersonic second-mode instability, which is likely to be dominant on smooth convex nearly-symmetric geometries with small cross-flow. Second-harmonic amplification was observed downstream, a good indication of nonlinear effects. A comparison of the second-harmonic amplification rate to a nonlinear computation would be interesting. A number of workers have already compared these results to computations; however, none have taken advantage of the substantial amount of tabulated data that is not presented in the conference papers. Although these are conventional-tunnel measurements with high ambient noise, the good-quality detailed measurements appear to deserve further computational comparisons.[5]

Brief Description of Experiments

The model was a 7 degree half-angle cone with a 40 inch (1.016 m) length and a sharp 0.0015 inch (38 micron) nose radius. The cone angle of attack was zero (within the accuracy with which this could be set and measured). The model was in thermal equi-

librium but heat conduction within the model may not be negligible.

Most of the measurements were carried out at a freestream Mach number of 7.95, with a total pressure of 225 psia (1.55 MPa) and a total temperature of 1310 R (728 K). Additional data was recorded at a lower total pressure (to determine the neutral-instability region) and at a higher pressure (to record data into transition onset). Thus, transition-onset data should be available.

Experimental data included surface pressure taps (24) and thermocouples (32), mean-flow profiles using pitot-pressure and total temperature probes and instability-wave spectra using calibrated constant-current hot-wire anemometry. Hot-wire measurements were recorded at one-inch (2.54-cm) intervals between 10 and 37 inches (25.4 and 94.0 cm), using a single hot-wire with a single calibration.

The experimental data is available on the RTO WG 10 SG 3 website (see above). See Schneider[5] for a detailed discussion.

Dataset No. 2: Blunt Cone at Mach 8

Prepared by

S. Schneider

Introduction

In addition to the sharp cone measurements in Dataset No. 1, Stetson *et al*[8, 9] carried out additional calibrated measurements of instability wave growth on several blunt cone models in AEDC Tunnel B at Mach 8. The apparatus was almost identical. This conventional wind tunnel is well characterized.[10] The blunt-cone experiments examined the effects of the entropy layer on the hypersonic second-mode instability. Herbert *et al*,[11] Kufner *et al*[12] and others have already compared some of these results to computations. Fig. 2 in Kufner *et al* summarizes the comparisons. All of the computations show a growth rate about 1.5 times the experimental value, at a frequency roughly 10% below the experimental value. However, these comparisons were carried out at a station 175 nose radii downstream of the tip. Fig. 7b in Stetson *et al*[9] paper shows substantial amplification of second-harmonic frequencies at this station. Stetson believes that nonlinearity is substantial at this station, therefore a growth-rate comparison to linear theory has dubious validity. Many workers have selected this station for comparison to linear theory, apparently through insufficient communication with Stetson *et al*.

The mean flow was measured for this experiment, but existing comparisons have uncovered some difficulties. Fig. 5 in Herbert *et al*[11] shows that an adiabatic-wall computation overpredicts the wall temperature by roughly 20%. This is thought to be due to heat transfer to the water-cooled sting support. While the measurements were carried out after thermal equi-

librium was achieved, heat transfer within the model apparently cannot be neglected.

Boundary-layer profiles were also measured using pitot and total-temperature probes. Unfortunately, repeated runs reveal discrepancies of 10-15% under nominally the same conditions (*e.g.*, Fig. 6 in Herbert[11]). Also, the data probably suffer from probe interference effects.[5]

The data show growth of the first and second-mode instability waves on a symmetric blunt cone under cold-flow conditions. The second-mode instability is dominant. Although amplification was only observed downstream of the nominal swallowing length, strong bluntness effects were apparent. Some entropy-layer fluctuations were also apparent, although these could not be resolved clearly and no quantitative comparisons have been attempted. Second-harmonic amplification of the second-mode waves was observed downstream, a good indication of nonlinear effects. A comparison of the second-mode amplification rate to a nonlinear computation would be interesting.

Description of Experiment

The model was a 7-degree half-angle cone with a 40-inch (1.016-m) length and a 0.15-inch (3.81 mm) nose radius. The cone angle of attack was zero, to within the accuracy with which this could be set and measured. The model was in thermal equilibrium but heat conduction within the model may not be negligible.

Most of the measurements were carried out at a freestream Mach number of 7.99, with a total pressure of 580 psia (4.00 MPa) and a total temperature of 1350 R (750 K).

Experimental data includes surface pressure taps (24) and thermocouples (32), mean profiles using pitot-pressure and total temperature probes, and instability waves using calibrated constant-current hot-wire anemometry. Hot-wire spectra were recorded at one-inch (2.54-cm) intervals between 10 and 31 inches (25.4 and 78.7 cm), with additional measurements at 33, 35, and 37 inches. Four hot-wires were used for these measurements, each calibrated separately. There is no data for transition onset on the blunt cone, according to Stetson.

AEDC carried out spectral analyses of the hot-wire data and printed out tables of amplitude *vs* frequency at these streamwise stations. These detailed experimental data are now available on the RTO WG 10 SG 3 website (see above). For a detailed discussion, see Schneider[5] and Kimmel.[13]

Suggested Approach

The following work seems to be warranted:

1. Use the existing wall-temperature data to perform mean-flow computations at isothermal conditions. Since no thermocouples exist forward of 7 nose

radii, it will be necessary to estimate the temperature distribution near the nose.

2. To obtain the experimental amplification rates, the experimental amplitude data were differentiated by AEDC. It seems preferable to integrate the computational amplification rates to compare amplitude ratios *vs* frequency between computation and experiment. Tabulated experimental data is available for this purpose, at the streamwise stations mentioned above.

3. Compare to the extensive mean-flow data. See if there is any consistent comparison between the computations and experiments.

4. Compare nonlinear computations to the amplification rates of the primary and 2nd-harmonic frequencies in the nonlinear region.

Dataset No. 3: Sharp Flared Cone at Mach 6

Prepared by

S. Schneider

Introduction

Three instability experiments[14-17] were carried out in the NASA Langley Mach 6 quiet tunnel before it was decommissioned. Due to schedule limitations, this is the only one with calibrated mean-flow profiles. The experiments were carried out on both sharp and blunt cones, but extensive data is available only for the sharp cone. All measurements were made using natural fluctuations, without controlled disturbance generators.

The first study that involved stability measurements of a laminar boundary layer in a quiet hypersonic tunnel was conducted by Lachowicz and Chokani in the early 1990s. As the constant voltage anemometer (CVA) was used to operate the hot-wire, and the CVA was poorly understood the stability analysis was derived from uncalibrated measurements. More recently our knowledge of the CVA has significantly improved; fortuitously also Lachowicz and Chokani did also conduct one systematic with a calibrated hot-wire. In the calibration, the hot-wire was operated at twelve overheats for seven mass flux/total temperature combinations. Then the calibrated hot-wire was used to examine the disturbance evolution on a sharp tipped cone flare model. On the model seventeen streamwise stations, each with thirteen points across the boundary layer were examined. At each measurement point the hot-wire is operated at seven overheats. This paper[18] describes and compares two methods for obtaining the calibrated data. In addition the effect of wire Reynolds number, overheat ratio, etc are also discussed. The paper shall be accompanied by a data report that tabulates the mean and rms profiles of mass flux and total temperature. These tabulated data may be useful for purposes of code validation.

The experiments[14-16] focused on the growth of first and second-mode instability waves on an axisymmetric cone under cold-flow conditions, in a quiet tunnel. An adverse pressure gradient exists on the rear half of the model. Second-mode amplification was observed. Görtler interactions are possible on the concave flare, although no experimental evidence is available.

Lachowicz *et al*[14] report agreement of 2-5% with linear-instabilty N-factor computations for the second-mode wave growth (*e.g.*, Fig. 9 in Lachowicz *et al*[14]). However, the ratio of CVA fluctuating voltages was taken as the ratio of wave amplitude. This assumption was used by Stetson and others for constant-current or constant-temperature anemometry, when the measurements were carried out with the hot wire at identical mean-flow conditions.

If this assumption can be verified, and any errors caused by it can be quantified, this dataset may be the best of the three. Although the aft end of the cone was outside of the fully quiet region, this is the only data obtained under quiet conditions. Static pressure data was obtained at three azimuthal positions to check angle of attack, although all boundary-layer measurements were again obtained on only one ray. The mean flow profiles are in fairly good agreement with existing computations.

These data were also obtained under equilibrium-wall temperature conditions. That is, the measurements were obtained only after the model-wall thermocouples reached steady-state temperatures. This occurred approximately 15-20 minutes after initiation of Mach-6 flow, following a subsonic preheat. Unfortunately, as for the Stetson data, this is not the same as adiabatic-wall conditions, for Chokani states that the heat-transfer within the model is not negligible.

Description of Experiment

The model was a 50.8 cm sharp cone. The first 25.4 cm formed a straight cone with a 5 deg half-angle. This was followed by a gentle flare with a 2.364 m radius of curvature. The profile shape is continuous; only the second derivative is discontinuous at the match point. The tip had a nominal radius of 2.5 microns. The cone angle of attack was nearly zero; however, most measurements were carried out at a yaw angle of approximately 0.1 deg. and a pitch angle of approximately 0.1 deg (see Lachowicz *et al*,[16] p. 20). Appendix D of Lachowicz *et al*[16] reports additional measurements carried out after additional efforts were made to align the model at zero angle of attack.

The measurements were carried out at Mach 5.91, with a total pressure of 896 kPa and a total temperature of 450K. The freestream Reynolds number was 9.25×10^6/m (note the typographical error in Lachowicz *et al*,[14] p. 2497).

Experimental data includes surface pressure taps (29) and thermocouples (51), mean flow profiles using

hot wires and CVA. Fluctuating profiles were obtained using same hot wires, but no calibrated fluctuations have so far been reported. See Riemann[18] for the latest information.

Suggested Approach

It is recommended that the reader contact Chokani or Schneider regarding the details of the experimental conditions and the available data. Further independent computations are needed, to see if the excellent agreement observed by Lachowicz *et al* can be repeated by others. Computations have been performed by Balakumar and Malik[19] and Pruett and Chang.[20] The computational approximations need to be evaluated. For example, computations should be carried out with an isothermal wall-temperature distribution adapted from the experimental data, to determine the effects of this boundary condition.

2. REAL GAS FLOWS
TEAM LEADER: G. CANDLER

Dataset No. 1: Circular Cylinder

Prepared by

W. Beck, G. Candler

Introduction

Hypersonic propelled flight will occur at Mach number from about four up to (perhaps) fifteen. Around the body of the vehicle at higher Mach numbers shocks are generated, behind which the air will be dissociated to different degrees, depending not only on the Mach number but also on the shock angle. Shock-shock interactions (*e.g.*, forebody-wing) can lead to locally very high heating rates. Shock boundary layer interactions, especially in the regions of body flaps, lead to influences on heating rates and body flap efficiency. The physical state and turbulence level of hot boundary layers, especially on the vehicle forebody upstream of its inlet and in its combustion chamber, are not fully understood. If, in addition to the above, the rôle of high temperature effects (especially chemical reaction) are added, then the picture becomes immensely difficult to measure experimentally and to calculate using CFD. The "real" vehicle case (fully 3-D geometry, possibly transitional flow or turbulence, full chemistry, complicated flow interactions) is too difficult a test case for examining the rôle of real gas effects.

Flows involving high temperature effects, especially kinetics, are generally high enthalpy, high temperature flows which are difficult to generate in a wind tunnel, which are even harder to characterize using the various available classical and optical diagnostic techniques, and which are complicated and not always amenable to CFD calculations. Some (but not all) of the difficulties encountered in carrying out aero(thermo)dynamic testing and in interpreting the data are: very short test times, contaminated flows (ablation material), nonstationary effects (nozzle start-up processes), driver gas arrival (in shock tunnels), incomplete characterization of the free stream (including knowledge of boundary layer transition), lack of accredited (qualified) kinetic data for CFD calculations, etc.

There are various kinetic schemes which have been used and further developed over recent years to examine air chemistry in high enthalpy flows. The validation of these schemes, with the consequent knowledge of having the correct scheme at the given conditions of temperature and pressure (*i.e.*, density) is considerably hampered by a lack of the type of high enthalpy data that is needed to distinguish between the different kinetic schemes. For example, it is easy to measure stagnation pressures on a model, but this result is virtually useless in distinguishing between kinetic schemes. More data are needed that probe the flow itself, preferably at the molecular level.

The approach suggested here is to simplify the problem as much as possible in order to focus on the high temperature effects. A circular cylinder flow has several advantages: line-of-sight symmetry (necessary for optical techniques), no complicated flow interactions (where the physics are only poorly understood, *e.g.*, unsteadiness, turbulence, transition, etc.), larger Δ/D (where Δ is the shock standoff distance and D is the cylinder diameter) than a sphere which simplifies the use of optical field measurement techniques, and quite straightforward to carry out CFD.

Description of Experiments

The experiments are in progress at HEG in DLR. The test case is a circular cylinder with diameter 90 mm and length (including shaped holder) 380 mm, placed with its axis transverse to the flow. The bow shock, generated in front of a circular cylinder placed in a flow with high total enthalpy, is strong enough to cause temperatures in the shock layer which are sufficient to bring about dissociation of oxygen and molecular nitrogen. Depending on the binary scaling parameter ρL (where ρ is the density and L is the characteristic length), the chemical relaxation processes will either reach equilibrium within the shock layer or will still be reacting (*i.e.*, remain in chemical non-equilibrium). Furthermore, the thermal behavior of the gas can also lead to non-equilibrium. Both high temperature effects, thermal and chemical non-equilibrium, lead to a modification of the gas properties (temperature, density, sound speed, etc.) behind the shock, which themselves lead to changes in shock properties such as shock standoff distance and shock shape.

Measurements (see below) on the cylinder have been carried out in HEG at high and intermediate total enthalpies (conditions I and III, ≈ 22 and ≈ 13 MJ/kg, respectively), at low pressures (nozzle reservoir ≈ 35

AMERICAN INSTITUTE OF AERONAUTICS AND ASTRONAUTICS PAPER 2002-0433

MPa) and with test gas air and nitrogen. Tests also at high pressures (100 MPa) are still under consideration.

The nominal HEG freestream data are listed in Table 4 for air at conditions I and III, based on a full Navier-Stokes turbulent non-equilibrium nozzle flow calculation (K. Hannemann) which uses experimental input such as shock speed, reservoir pressure and nozzle wall heat transfer in order to calculate the nozzle exit conditions (K. Hannemann, M. Schneider) as given below:

Table 4   Circular Cylinder

Reservoir	Cond I	Cond III
Pressure p_0 (MPa)	35	44
Temperature T_o (K)	9120	6980
Specific enthalpy (MJ/kg)	21.7	12.5
Freestream		
Pressure p_∞ (Pa)	660	790
Density ρ_∞ (kg/m^3)	0.0017	0.0033
Temperature T_∞ (K)	1140	810
Pitot pressure p_{t_2} (kPa)	55.4	66.1
Mach number M_∞	8.17	8.14
Flow velocity U_∞ (m/s)	5940	4660
Freestream mass fractions		
$[N_2]$	0.745	0.731
$[O_2]$	0.047	0.171
$[NO]$	0.0293	0.059
$[N]$	4.6×10^{-9}	1.3×10^{-10}
$[O]$	0.178	0.038

The chemical kinetic scheme uses the Park model. CFD results are validated by comparison with measured values of p_o, p_∞, ρ_∞, T_∞, p_{t_2}, q_{t_2} and U_∞.

The cylinder is equipped with pressure and temperature sensors at various positions (angles) along its arc length. Freestream static and Pitot (small sphere) pressures and stagnation heat transfer (small sphere) are recorded each run for calibration, normalization and statistical purposes. Flow visualization around the cylinder is carried out with the Schlieren and holographic interferometric techniques. The use of further techniques (spectroscopic techniques such as PLIF) must await further development and successful implementation.

Dataset No. 2: Shock-Shock Interaction on Cylindrical Leading Edge

Prepared by

M. Holden

Introduction

In his early studies of shock-shock interaction, Edney speculated that regions of shock-shock interaction should be strongly influenced by real gas effects which should significantly enhance heat transfer and pressure levels in the interaction region by changing the shock structure in the shock-shock interaction. However, preliminary studies in high enthalpy flows at GALCIT and in the HEG facility in Germany indicated that real gas effects caused a decrease in both the heat transfer and pressure amplification factors. The low spatial and temporal resolution of the instrumentation employed in these studies, coupled with the data reduction methods may have had a significant influence on the accuracy of this data. Again, the question of the laminar or transitional nature of the phenomena has also been raised. Subsequently, experimental studies of shock-shock interaction phenomena were conducted in the LENS facility employing models with high spacial resolution and a sufficient frequency response to accurately define the distribution of heat transfer and pressure in the interaction region. Measurements were made in both air and nitrogen flows and these studies indicated that real gas effects resulted in a significant enhancement of the amplification factors in the interaction regions. These studies were followed by measurements on a cone-cone configuration which also indicated increased amplification factors as a result of real gas effects in regions of shock-shock interaction.
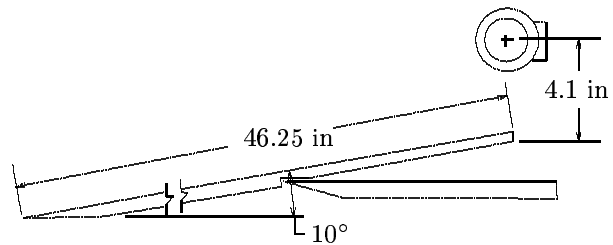

Fig. 1   Type IV interaction

Description of Experiments

The configuration is shown in Fig. 1. An inclined flat plate generates a two dimensional oblique shock wave which interacts with the bow shock generated by the 1.5 in radius cylinder. The characteristic of the shock-shock interaction depends on a variety of parameters including the relative shock strengths and positions of the oblique and blunt body shocks and these effects were explored in the experimental program. Experiments were performed for cylinder radii of 0.375 and 1.5 in. The experimental data[21–23] includes surface temperatures, heat transfer and pressure distributions. The freestream conditions are shown in Table 5 and the reference CD-ROM.[23]

Table 5   Shock-Shock Interaction

M_∞	Re (ft^{-1})	Driven Gas	Enthalpy (MJ/kg)	Run No.
8.615	1.386×10^5	Air	11.3	50
9.278	1.612×10^5	N_2	10.5	48

Dataset No. 3: Blunt 25° Cone/60° Flare (Indented Nose) Configuration

Prepared by

M. Holden

Introduction

Earlier experimental studies with indented nose tips by Holden and more recently computations performed by Candler have suggested that the flow structure over, and the aerothermal loads generated on a blunted cone-cone configuration, similar to that of an idealized indented nose tip, can be sensitive to real gas effects. Originally indented nose shapes were studied because of an interest in the development of ablated nose tips, similar to those generated with graphite nose tips during ballistic reentry. Later Candler, in numerical studies designed to select configurations which were sensitive to real gas effects, suggested a cone-cone configuration similar to those studied earlier by Holden. To further investigate real gas effects on flowfield structure and surface properties, Holden designed a blunted cone/flare configuration which was highly instrumented with high-frequency heat transfer and pressure gages. Measurements were attained to provide distribution of the surface properties as well as information on any high-frequency flow oscillations that may arise. Test conditions weres selected to obtain air and nitrogen freestream flows at enthalpies of 5 and 10 MJ/kg at reservoir pressures of 270 to 500 bars. Computations employing the Navier-Stokes code have been made by Candler and Gnoffo to examine both these flow configurations. These computations suggested that the flows were unstable, a feature not observed in the experiment. The numerical results were also highly grid-sensitive and caused significant debate and controversy in the Navier-Stokes solver community.
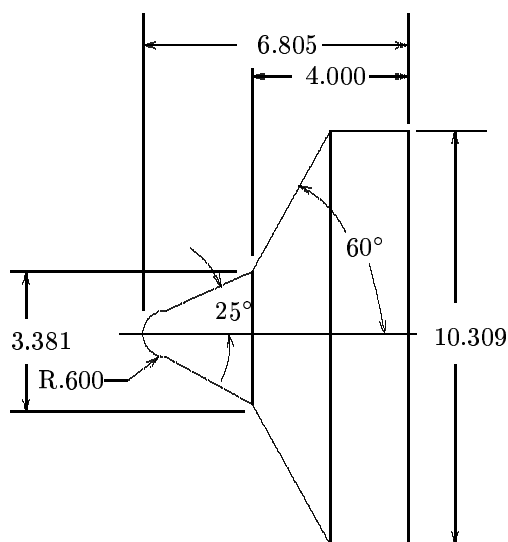

Fig. 2   Blunt cone (60°) (dimensions in inches)

Description of Experiments

The experiments were performed at Calspan - University at Buffalo Research Center (CUBRC) and are described in Holden.[23-25] The configuration is a 25° cone with a 60° flare, and is shown in Fig. 2. The experimental data includes surface temperatures, heat transfer and pressure distributions. The freestream conditions are shown in Table 6 and the reference CD-ROM.[23]

Table 6   Sharp-nose Cone-Flare

M_∞	Re (ft^{-1})	Driven Gas	Enthalpy (MJ/kg)	Run No.
8.439	1.481×10^5	Air	11.4	43
8.623	1.379×10^5	Air	11.3	46
9.279	1.563×10^5	N_2	10.5	45
10.49	3.791×10^5	N_2	5.8	44
10.60	3.774×10^5	Air	5.5	42

Dataset No. 4: Large Spherically Blunt-Nose Cone-Flare

Prepared by

M. Holden

Introduction

Two sets of studies were conducted with the large blunt nose cone-flare configuration. This model was highly instrumented with heat transfer and pressure gages to obtain detailed surface distributions for a range of freestream conditions at velocities between 10,000 ft/sec and 15,000 ft/sec for both nitrogen and air flows. The electron beam and the associated pneumatic and electrical apparatus, together with photomultiplier detection systems, were also installed into the model. A higher density of surface instrumentation was employed in the immediate vicinity of the cone-flare junction to detect and quantify the presence of a laminar separated region. The flare region was also densely instrumented to accurately quantify the reattachment compression region. Measurements of the distribution of heat transfer and pressure over the model were obtained for total enthalpy conditions of 5 MJ/kg and 10 MJ/kg, with reservoir pressure of 500 bars, with both nitrogen and air used as the test gas. These conditions were selected to explore the effects of the Reynolds number, which influences the occurrence of transition and total temperature and pressure and influences the flow chemistry.

Description of Experiments

The configuration is a 15° cone with a 30° flare and an indented nose, which is presented in Fig. 3. The experimental data[24, 25] includes surface temperatures, heat transfer and pressure distributions. Flowfield surveys were also performed to examine real-gas effects on shock position close to the sphere/cone junction. The
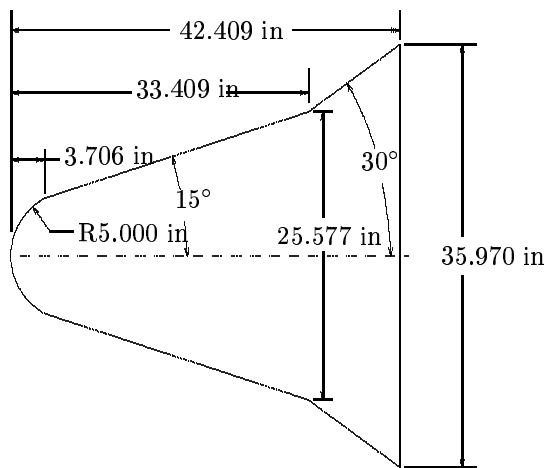
Fig. 3   Large spherically blunt nose cone-flare

freestream conditions are shown in Table 7 and the reference CDROM.[23]

Table 7   Blunt-nose Cone-Flare

M_∞	Re/ft $(\times 10^5)$	Driven Gas	Enthalpy (MJ/kg)	Run No.
8.508	1.474	Air	11.2	61
9.404	1.519	N_2	10.5	60
10.55	3.920	N_2	5.7	59
10.58	4.083	Air	5.4	63

3. LAMINAR VISCOUS-INVISCID INTERACTIONS
TEAM LEADER: M. HOLDEN

Dataset No. 1: Hollow Cylinder Flare

Prepared by

T. Pot, B. Chanetz.

Introduction

This test case is proposed for Navier-Stokes solvers validation in the field of high speed flows characterized by axisymmetric strong shock-wave boundary-layer interaction in the fully laminar flow regime. The experiment was carried out in the R5Ch blow-down Hypersonic Wind Tunnel in the Fundamental and Experimental Aerodynamics Department of ONERA headed by Prof. J. Délery, France. Further numerical studies (code-to-code comparison) and comparison with experimental data have been performed once in the frameworks of AGARD Working Group 18, then of the first Europe-US data base and the first Eastern-Western High Speed Flow Field data base. Details are presented in Chanetz et al.[26–28]

Description of Experiments

The model is comprised of a hollow cylinder with an external diameter of 65 mm and an internal diameter of 45 mm as shown in Fig. 4. The leading edge is sharp with an angle of 15°. A 30° flare is located 101.7 mm

downstream of the cylinder leading edge. The flare is followed by a cylindrical part having a diameter of 115 mm and a length of 25 mm. The advantage of this configuration is twofold: i) to put baseflow far enough downstream of the interaction region, and ii) to eliminate three dimensional effects. The origin of the coordinate system is located at the leading edge of the hollow cylinder. The mesh coordinates are nondimensionalized by the reference length $L = 0.1017$ m. The test conditions (Table 8) are perfect gas ($\gamma = 1.4$), axisymmetric, fully laminar flow, laminar viscosity by Sutherland's Law. Experimental data includes surface pressure coefficient distribution, surface heat transfer (Stanton number) distribution, surface oil-flow visualization (skin friction lines), flowfield visualization by the Electron Beam Fluorescence (EBF) technique, and density profiles.
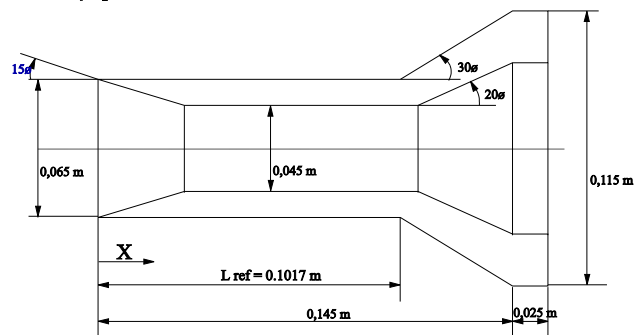

Fig. 4   Hollow cylinder flare

Table 8   Hollow Cylinder Flare

Quantity	Value
M_∞	9.91
Re/m	1.86×10^5
T_∞	51 K
p_∞	6.3 Pa
T_{wall}	293 K
L	0.1017 m

Dataset No. 2: Hollow Cylinder Flare

Prepared by

M. S. Holden

Introduction

This study was conducted to obtain detailed experimental measurements of the heat transfer and pressure distribution over two cylinder-flare models, one of which replicates a configuration employed earlier in French code validation experiments (see above) and a second which employs a longer flare to obtain a better defined downstream boundary condition. The boundary layer was laminar over the entire cylinder-flare surface in all cases, thereby enabling a detailed comparison between DSMC, Navier Stokes and hybrid codes. A detailed description of the experiments is presented in Holden and Wadhams.[29]
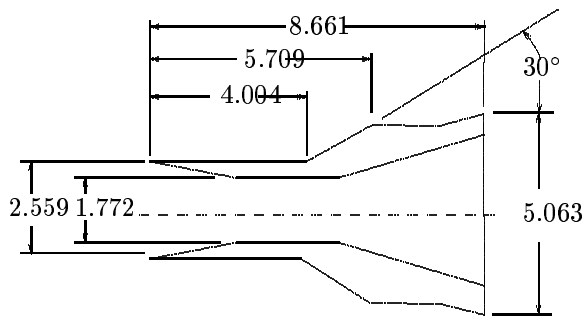
Fig. 5 Hollow cylinder with short flare (dimensions in inches)
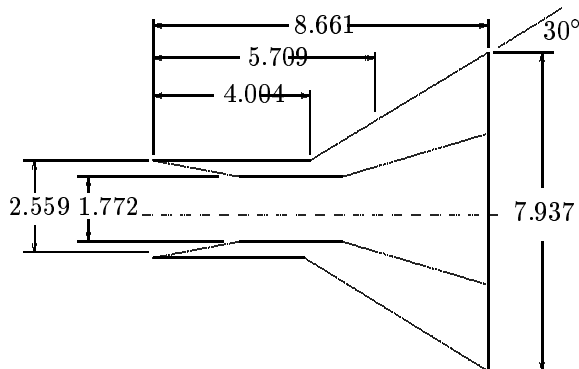

Fig. 6 Hollow cylinder with long flare (dimensions in inches)

Description of Experiments

The two model configurations are shown in Figs. 5 and 6. The first configuration employs a shorter flare configuration which is identical in geometry to the configuration used in earlier French code validation experiments. Because we had believed that the separated region on this configuration is influenced by the expansion at the downstream end of the conical flare, we had requested P. Gnoffo (NASA Langley) perform calculations to determine the length of flare required to ensure that the separated region is not effected by the shoulder and region of constant pressure generated upstream of the end of the flare. Based on results of Gnoffo's calculations, we selected the second of the two configurations (Fig. 6), which has a flare of sufficient length so that the separated region is uninfluenced by the downstream end of the conical flare. These two model configurations were employed in studies at Calspan at the test conditions indicated in Table 9. The test conditions were selected on the basis of many flowfield calibration studies to ensure streamwise and lateral flowfield uniformity. The experimental measurements include detailed high frequency surface temperatures, heat transfer and pressure distributions and Schlieren photographs of the flow.

The flowfield physics for this study consist of perfect gas, axisymmetric flowfield, fully laminar shock wave-boundary layer interactions, and flow separations. The test gas is nitrogen.

Table 9 Hollow Cylinder

Flare	Case	M_∞	Re/ft $(\times 10^4)$
Short	1	9.30	10.8
	2	9.44	8.33
	3	11.3	6.28
	4	11.4	10.7
	5	11.5	7.92
Extended	1	9.33	10.9
	2	9.38	6.51
	3	9.45	7.89
	4	9.50	5.60
	5	11.1	4.75
	6	11.4	7.19
	7	11.4	7.89
	8	11.4	10.7

Dataset No. 3: Sharp-Nose and Blunt-Nose Cone-Flare (Indented Nose) Configuration

Prepared by

M. Holden, G. Candler, J. Harvey

Introduction

The flows around hypersonic vehicles will have regions of shock/shock and shock/boundary layer interaction which can induce embedded regions of separated flows over, for example, control surfaces, and in and ahead of airbreathing ramjet or scramjet engines. Oblique shock waves generated inside the engine can also cause extensive regions of three dimensional boundary layer separation.

Recent work has shown that the flow generated by a cone-flare geometry is very challenging to compute. This flow, with an attached leading edge shock and a detached bow shock from the second cone, produces a complicated interaction between the shock waves and the separation zone. The size of the separated region is very sensitive to the shock angles and the strength of the shock interaction. Because the size of separated region can be measured with surface measurements and with flow visualization methods, this flowfield is an excellent test case for code validation. Also, because the flow is axisymmetric, the flowfields require only two-dimensional simulations.

The cone-flare configuration is a challenge for CFD because it is critical to resolve the initial boundary layer growth near the model leading edge. Additionally, the shock interaction must be captured accurately in order to correctly predict the interaction between the shock waves and the separation zone. However, Wright *et al*[30] have shown that sufficiently fine grids and careful grid generation CFD methods can reproduce this type of flowfield. The more challenging higher cone angle cases given in Wright *et al* have a transitional shear layer, and as a result are not suitable for benchmark CFD validation studies. Therefore

a new set of experiments with purely laminar flow has been designed and performed at Calspan by M. Holden. The models are heavily instrumented to accurately locate the separation and reattachment points. The experiments were selected on the basis of earlier studies in separated flows to ensure that the flows over the cone-flare configurations will remain laminar throughout the interaction region.
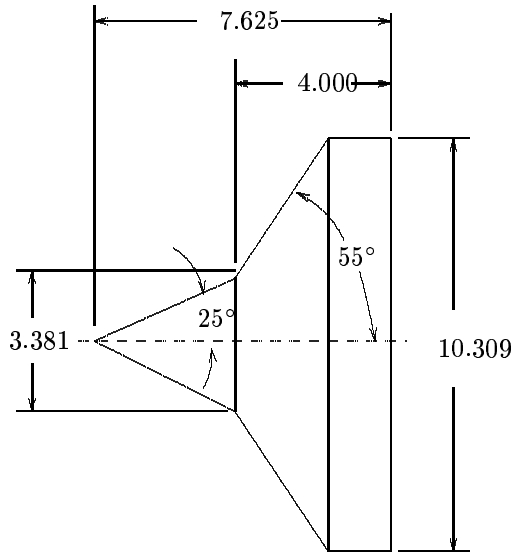
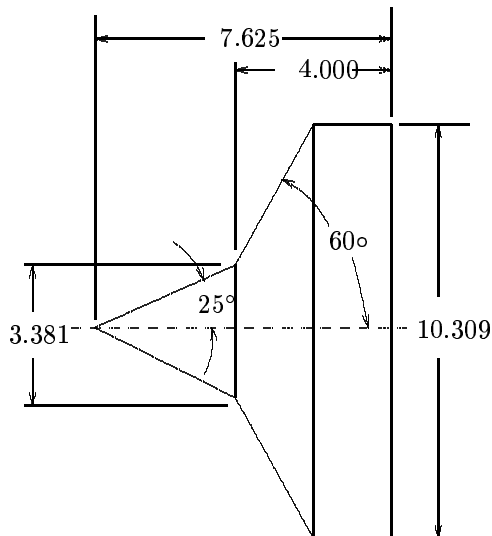Fig. 7   Sharp cone (55°) (dimensions in inches)

Fig. 8   Sharp cone (60°) (dimensions in inches)

Fig. 9   Blunt cone (55°) (dimensions in inches)

Fig. 10   Blunt cone (60°) (dimensions in inches)

Description of Experiments

Several of the model configurations are shown in Figs. 7, 8, 9 and 10. A full description of the models is provided in Holden and Wadhams.[29] The blunted 25° cone with a 60° flare was employed in earlier experimental studies with the objective of investigating the effects of real gas on flowfield geometry. These experimental studies indicated that the flowfield was steady, and that there were significant differences be-
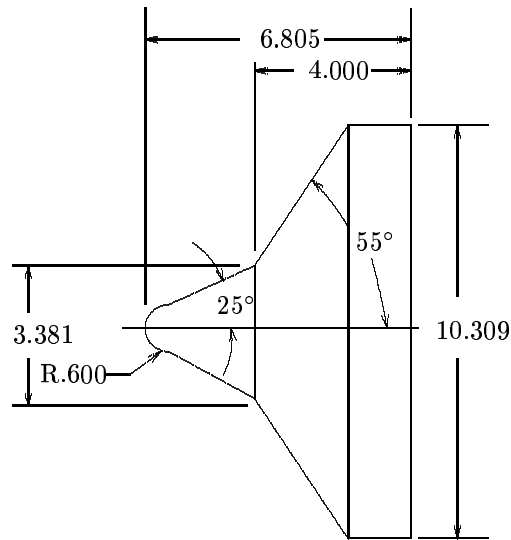
tween the heat transfer and pressure distributions for nitrogen and air flows. However, computations by G. Candler and P. Gnoffo indicated that the flows over this configuration are unsteady, and grid refinement studies indicated the solutions were grid dependent. We repeated the experiment at much lower Reynolds numbers (see Table 10) to ensure that the flow remains completely laminar throughout the interaction region over this configuration.

We investigated the effect of nose bluntness by employing a sharp 25° nosetip. In addition, we performed studies with the blunt and sharp nosetips with a 55° conical flare in place of the original 60° flare. The 55° flare configuration was selected in conjunction with calculations done by P. Gnoffo, which indicated that the basic flow over the configuration was stable, although there appeared to be some problems in regards to instability in the recirculation region.

A bow shock is generated over the sharp or spher-

ically blunted nosetip which interacts with the detached bow shock generated over the flare. A region of shock/shock interaction is generated at the intersection of the two shocks and the resultant shock/-boundary interaction induces an embedded separated region at the cone/flare junction. The coupling between the shock/shock interaction and the separated zone makes this flow very sensitive to grid refinement in numerical simulations. The computed flowfield is also very sensitive to the grid spacing at the nosetip and in the reattachment compression region at the base of the shock/shock interaction.

Table 10   Sharp- and Blunt-Nose Cone-Flare

Cone-Flare	Nose Radius (in)	M_∞	Re/ft $(\times 10^4)$
25°/55°	sharp	9.42	6.18
		9.48	7.79
		9.59	4.25
		11.3	4.76
	0.250	9.42	6.27
		9.43	7.26
		9.56	4.34
		11.3	4.33
	0.288	9.42	6.41
		11.5	4.18
	0.600	9.47	3.80
25°/60°	sharp	11.4	4.70
	0.250	11.3	4.44

The experimental data include detailed heat transfer and pressure distributions. The 55° model is instrumented with 20 pressure gauges and 34 temperature gauges while the 60° model is instrumented with 18 pressure gauges and 33 temperature gauges in the separation and reattachment locations. Measurements were performed with both the blunt and sharp double cones for flare angles of 55° and 60°. The freestream conditions are shown in Table 10. The test gas is nitrogen.

4. SHOCK-SHOCK INTERACTIONS
TEAM LEADERS: J. SCHMISSEUR
S. WALKER

Dataset No. 1: Shock-Shock Interaction

Prepared by

T. Pot, B. Chanetz

Introduction

This problem has been proposed to evaluate CFD codes for the analysis of complex shock-shock interactions. The interaction between an impinging shock wave generated by a wedge and the bow shock around a circular cylinder (Type IV shock-shock interaction in the classification of Edney) is considered. The experiments were conducted in the R5Ch in the Fundamental and Experimental Aerodynamics Department of ONERA headed by Prof. J. Délery, France. Details are presented in Pot *et al*,[31] Moss *et al*,[32] Délery and Chanetz[33] and Reijasse *et al*.[34]

Description of Experiments

The arrangement of the cylinder and the wedge models in the test section is shown in Fig. 11. The relative locations of the cylinder and the wedge are selected in order to obtain a Type IV shock-shock interaction. The wedge angle is 20° and the wedge length is equal to Lwedge = 0.1 m. Its span is 0.1 m. The axis of the cylinder is perpendicular to the free stream direction. The distance between the leading edge of the shock generator and the cylinder center is 0.11 m along the x-axis (longitudinal parallel to the upstream flow direction) and 0.053 m along y-axis (perpendicular to the upstream flow direction). The origin of the coordinate system is located at the nose of the cylinder. The mesh coordinates are nondimensionalized by the cylinder radius $R_{\rm cyl} = 0.008$ m.
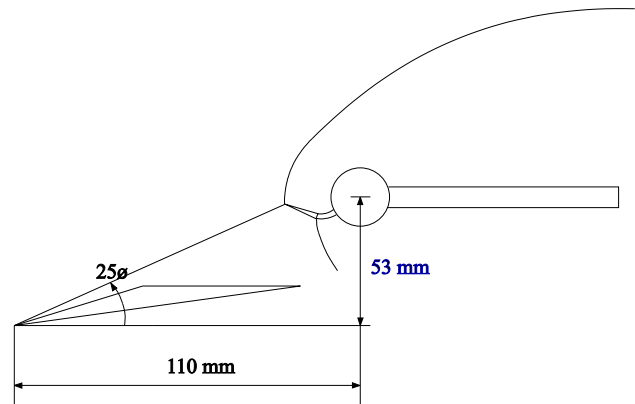

Fig. 11   Type IV interaction

Table 11   Shock-Shock Interaction

Quantity	Value
M_∞	9.91
Re/m	1.86×10^5
T_∞	51 K
p_∞	6.3 Pa
$T_{\rm wall}$	293 K
L	0.1017 m

The flowfield is described as a perfect gas ($\gamma = 1.4$), two-dimensional, fully laminar flow, and laminar viscosity by Sutherland's Law.

The cylinder is equipped with thermocouples and pressure taps. The experimental data includes wall pressure, wall heat flux, flowfield visualization by the Electron Beam Fluorescence technique, and density and temperature measurement in the flowfield interaction (more than 100 data points).

The selected flow conditions are listed in Table 11. The effective stagnation conditions ($p_{t_\infty} = 2.5 \times 10^5$

Pa and $T_{t_\infty} = 1050$ K) yield the freestream properties shown in the Table.

Dataset No. 2: Shock-Shock Interactions For Ideal Gas Flows

Prepared by

M. S. Holden

Introduction

An extensive series of studies[23, 25, 35, 36] was conducted over a range of Mach numbers from 10 to 16 to define the aerothermal loads generated in regions of shock-shock interaction from the rarefied flow to the fully continuum turbulent flow regimes. Detailed heat transfer and pressure measurements were made in the 48-inch, 96-inch and LENS shock tunnels. The results of these studies were analyzed to provide guidance to predict the heating enhancement factors in laminar transitional and turbulent flow regimes. The test conditions presented here (Run Nos. 36, 38, 39, and 40) is a subset of the experiments for fully laminar flows; for all but one test condition, where the flows in the interaction region are "fully" turbulent.
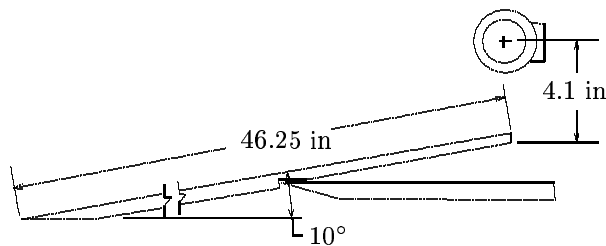

Fig. 12   Type IV interaction

Description of Experiments

The model configuration is shown in Fig. 12. The regions of shock-shock interaction studied were generated over a series of cylindrical leading edge configurations with nose radii of 0.138, 0.375, and 1.5 inches. Each of these leading edges was densely instrumented with heat transfer instrumentation placed to have a circumferential resolution within one degree. The thin-film instrumentation was deposited on a low-conductivity surface to minimize measurement errors associated with lateral conduction in the large heat transfer gradients generated in the region of peak heating. The high-frequency response of the thin-film instrumentation was also a key factor in accurately determining the heating distribution for shock-shock interactions, which exhibited intrinsic flow unsteadiness.

The flowfield physics for this study consist of perfect gas, planar flowfield, shock-shock interactions, fully laminar and highly turbulent flows.

The experimental data includes surface temperature, heat transfer and pressure distributions and Schlieren photographs. A sample of freestream test conditions is shown in Table 12. Additional information is available in Holden.[23]

Table 12   Shock-Shock Interaction

Runs	36	38	39	40
M_i	5.675	5.534	5.490	5.517
$p_0 \times 10^{-2}$ (psia)	4.568	4.659	4.097	4.201
$H_0 \times 10^{-7}$ (ft^2/s^2)	4.686	4.451	4.401	4.439
$T_0 \times 10^{-3}$ (°R)	5.987	5.784	5.731	5.767
M	13.99	14.15	14.17	14.15
$U \times 10^{-3}$ (ft/sec)	9.561	9.319	9.268	9.308
T (°R)	193.5	179.9	177.2	179.4
$p_\infty \times 10^4$ (psia)	5.324	5.312	4.657	4.788
$\rho_\infty \times 10^7$ (slug/ft^3)	2.298	2.467	2.195	2.230
$\mu_\infty \times 10^7$ (slug/ft-sec)	1.560	1.449	1.427	1.444
$Re \times 10^{-4}$ (ft^{-1})	1.409	1.587	1.426	1.437
$p_0' \times 10^1$ (pitot) (psia)	1.339	1.366	1.202	1.232

Dataset No. 3: Steady Shock Wave Reflection Transition and Hysteresis

Prepared by

M. Ivanov, A. Kudryavtsev, D. Khotyanovsky

Introduction

The intersection of two symmetric oblique planar shock waves results in either a Regular Reflection (RR) or Mach Reflection (MR) depending on the upstream Mach number and shock angle as illustrated in Fig. 13. At sufficiently high Mach numbers, three regimes exist delineated by α_N (the von Neumann criterion) and α_D (the detachment criterion) as shown in Fig. 14. For incident shock angle $\alpha < \alpha_N$, only RR is possible, and for $\alpha > \alpha_D$ only MR is possible. In the region $\alpha_N < \alpha < \alpha_D$ (the dual solution domain) both types of reflection are theoretically possible. It was hypothesized by Hornung that a hysteresis phenomenon should be observed when changing the incident shock wave angle continuously, *i.e.*, the transition from RR to MR should occur at $\alpha \approx \alpha_D$ and reverse transition from MR to RR at $\alpha \approx \alpha_N$. The hysteresis was first obtained numerically by Ivanov *et al.*[37] Recently, experiments by Ivanov *et al.*[38] have confirmed the hypothesis of Hornung.
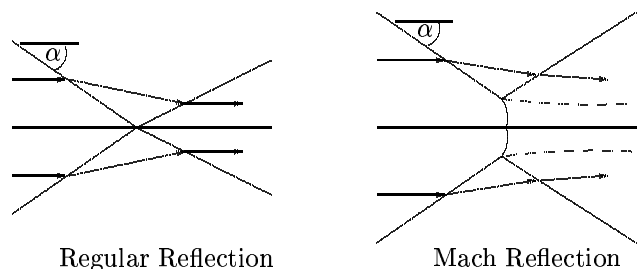

Regular Reflection   Mach Reflection

Fig. 13   Regular and Mach reflections

The test case proposed is to perform unsteady 2D Euler simulations of shock wave reflection in the dual solution domain, to determine the angles of the tran-
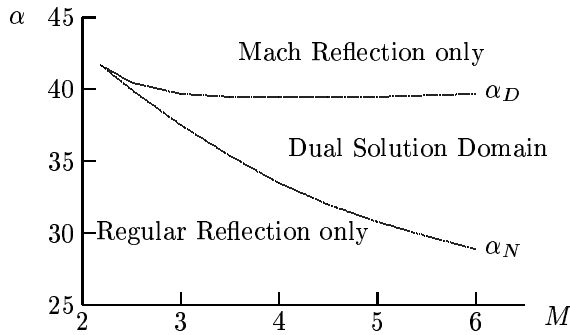
Fig. 14   Dual solution domain

sition from RR to MR, and back, and to obtain numerically the hysteresis in simulations with increasing and decreasing the incident shock wave angle. At first stage, only 2D computations are proposed.

This problem is very attractive in terms of verification of the available numerical codes for solving Euler equations. The numerical simulation of the transition from RR to MR is a challenging task for various CFD methods because of the following features present in the flow: strong shock waves, low density regions behind the wedge, possible unsteady phenomena such as the instability of a slip surface at MR; importance of accurate prediction of the angles of the transition between RR and MR; existence of two stable states (RR and MR), and hysteresis.

Description of Experiments

Two symmetrically-spaced 15° wedges are installed in a supersonic flow at the angle of attack θ. Incident shock waves generated by either wedge interact near the plane of symmetry. This symmetrical arrangement allows to eliminate viscous effects inevitable at shock wave reflection from the wall. Figs. 15 and 16 give the schematic of the flow for RR and MR: IS (incident shock), RS (reflected shock), EF (expansion fan), MS (Mach stem), SS (slip surface), P (reflection point), and T (triple point). The flowfield is a perfect gas ($\gamma = 1.4$), inviscid two-dimensional flow, with shock wave reflection transition.
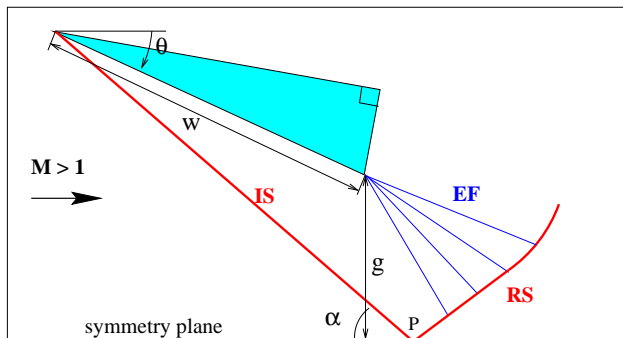

Fig. 15   Regular reflection

All the lengths are non-dimensionalized by the wedge length w. The distance between trailing edge of the wedge and the plane of symmetry is chosen to
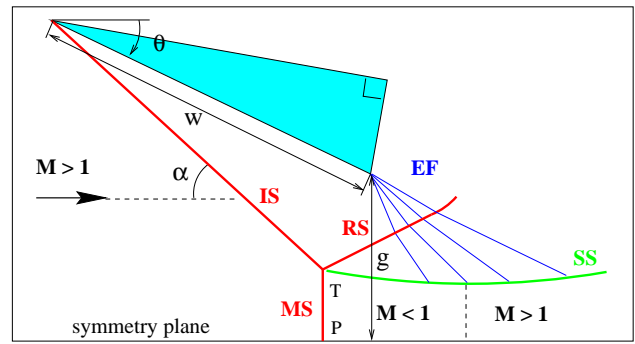

Fig. 16   Mach reflection

be $g/w = 0.42$ to provide clear conditions when the reflected shock at MR does not impinge on the wedge surface (which results in a choked flow) even at large incident shock angles, and, on the other hand, the expansion fan does not interact with the incident shock. The wedge is rotated around its trailing edge (*i.e.*, g/w is kept constant), thus changing its angle of attack θ, and correspondingly the incident shock angle α. The angles of the transition $\alpha_{RR \to MR}$, $\alpha_{MR \to RR}$ between RR and MR may be compared with theoretical criteria, and the results computed by various codes. The Mach stem heights at MR at various α may also be compared with experiment.

Experiments[39] were conducted at ITAM T313 facility at $M_\infty = 4$ and 5. At $M_\infty = 5$, the corresponding theoretical criteria are $\alpha_N = 30.79°$, $\alpha_D = 39.33°$. The experimental data include the Mach stem heights measured at different α, Schlieren visualizations, and laser sheet patterns. The relative spanwise extent of the wedge was varied from $b/w = 0.66$ to $b/w = 3.75$ in these experiments. The experiments were made at the Reynolds number based on the free-stream parameters and the length of the wedge $Re_w = 2 \times 10^6$, i.e. the wedge boundary layer effects can be neglected and Euler simulations are justified in this case.

Previous simulations by Ivanov *et al*[37,40] were made in the following manner. For the incident shock wave angle α near and slightly below the von Neumann condition α_N, a RR was obtained. Using this RR field as the initial data, the angle of the wedge θ was increased until the transition from RR to MR occurred at the incident shock angle $\alpha_{RR \to MR}$ (which is near and slightly above α_D). After that, with the obtained MR configuration as the initial data, the angle of the wedge was decreased down to α_N, near which at $\alpha = \alpha_{MR \to RR}$ the transition to RR should occur. The computations thus covered the whole dual solution domain and the hysteresis loop was obtained during decreasing and increasing the incident shock angles. The transition angles in the computations are very grid-sensitive, and are also dependent on the numerical viscosity. Mach stem heights correspond well with the experimental ones, except at large α where 3D effects become more pronounced in the experiments.

Dataset No. 4: 3D Steady Shock Wave Reflection

Prepared by

M. Ivanov, A. Kudryavtsev, D. Khotyanovsky

Introduction

The investigation of the nature of the transition between RR and MR of steady shock waves between two wedges is incomplete without a consideration of three-dimensional effects on shock wave configuration. A finite spanwise extension of a test model may have an important influence on the experimental results. Incident shock waves become non-planar because of their interaction with an expansion flow generated by lateral edges of the wedges. It is clear that, depending on the geometrical sizes, the shock wave interaction may be purely 3D or contain a portion where the incident shock waves remain planar. In the case of MR, a subsonic region behind the Mach stem exists, and as a result, the central plane flow should be influenced by the 3D effects. Strictly speaking, the existing theoretical criteria of transition between RR and MR cannot be applicable to real 3D flows.

The conventional Schlieren experimental technique gives flow images integrated along the spanwise direction and, consequently, does not allow us to investigate the 3D structure of shock wave configurations. The laser sheet method has been utilized by Ivanov *et al*[41] to obtain the series of spanwise slices and reconstruct the whole 3D flow patterns.

Numerical modelling can provide much more detailed information concerning the 3D structure of shock wave reflection. The test case proposed is to perform the 3D Euler simulations of the RR and MR of steady shock waves generated by two symmetrical wedges of finite spanwise extension. The comparison of numerical and experimental data gives an opportunity to validate numerical codes for simulation of supersonic flows with complicated 3D shock wave interactions and investigate this challenging problem having great theoretical and practical importance.

Description of Experiments

Two symmetrically spaced wedges, which have the angle 15°, are installed in a uniform supersonic stream at the angle of attack θ and generate two interacting oblique shock waves. This symmetrical arrangement allows us to eliminate viscous effects inevitable at shock wave reflection from the wall. The flowfield is a perfect gas ($\gamma = 1.4$), inviscid 3D flow, steady shock wave reflection.

Fig. 17 gives the schematic of the test model and the sketch of shock wave configuration in the vertical plane of symmetry. Here IS is the incident shock, RS is the reflected shock, MS is the Mach stem, SS is the slip surface emanating from the triple point T, h and g denote distances from the horizontal plane of symmetry to the leading and trailing edges of the

wedge, respectively, w is the wedge length, b is its span, and s is the half-height of the Mach stem.
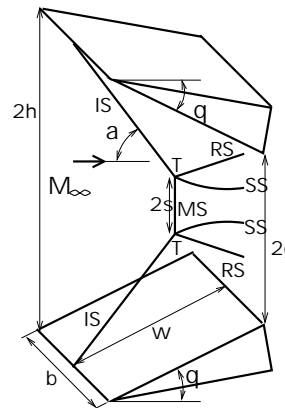

Fig. 17 3-D shock wave reflection

Experiments[41, 42] were conducted at ITAM T313 blow-down wind tunnel at a freestream Mach number $M_\infty = 4$. The experimental data include the Mach stem heights measured at different α, Schlieren visualizations, and laser sheet patterns taken in different spanwise cross-sections.

The relative span of the wedge in these experiments was varied from $b/w = 0.66$ when the incident shocks in the vertical plane of symmetry are affected by the lateral expansions to $b/w = 3.75$ when the shocks in the central part of the flow were planar. The experiments were made at the Reynolds number based on the free-stream parameters and the length of the wedge $\text{Re}_w \sim 2 \times 10^6$, *i.e.*, the wedge boundary layer effects can be neglected and Euler simulations are justified in this case.

Previous Simulations

Previous 3D simulations by Ivanov *et al*[43] and Kudryavtsev *et al*[44] were performed both with Euler code and DSMC method for different flow parameters and geometries. The computations revealed the hysteresis phenomenon at the transition from RR to MR and back, similar to that observed earlier in 2D case. The Mach stem heights in experiments and computations are in excellent agreement, and strong dependence of the Mach stem height on the wedge span is confirmed. A close resemblance of numerical and experimental flow patterns was shown with the help of numerical Schlieren pictures integrated along the spanwise coordinate as well as by comparison of the numerical and experimental (laser-sheet) slices at different spanwise locations. New and surprising details of the 3D shock wave configurations were revealed at first numerically and then confirmed experimentally. These details include the peripheral MR when the overall configuration is regular, the non-monotonic variation of the Mach stem height in the spanwise direction at the MR, and the shock wave configuration with intermittent type of reflection: MR/RR/MR.

5. SHOCK WAVE TURBULENT BOUNDARY LAYER INTERACTIONS TEAM LEADER: D. KNIGHT

Prepared by

D. Knight, A. Panaras, A. Zheltovodov

Introduction

The Conventional Reynolds-averaged Navier-Stokes (CRANS) methods[i] have typically been unsuccessful in predicting several of the important aerodynamic and aerothermodynamic properties of shock wave turbulent boundary layer interactions (also denoted as "interactions") with strong flow separation. CRANS methods do not accurately predict the observed mean surface pressure, skin friction and heat transfer in nominally two dimensional separated interactions.[45–48] CRANS methods do provide accurate predictions of surface pressure for many moderately separated three dimensional interactions, but do not provide an accurate prediction of skin friction and heat transfer for separated interactions.[45–49] Additionally, CRANS does not provide rms fluctuating surface pressure.

The inability to accurately predict the desired aerodynamic and aerothermodynamic properties of shock wave-turbulent boundary layer interactions significantly degrades the capability for design of effective hypersonic vehicles. Research in the development of new methodologies for accurate prediction of these flows is critically important to the development of the next generation of hypersonic vehicle designs.

Three approaches have recently been identified as promising candidates for improving prediction of shock wave turbulent boundary layer interactions – specifically, for achieving improved prediction of aerodynamic and/or aerothermodynamic properties compared to CRANS methods. The first approach is Direct Numerical Simulation (DNS) wherein the entire spectrum of turbulent fluctuations is resolved in the simulation. The second approach is Large Eddy Simulation (LES) wherein the large energy-containing eddies are explicitly computed and the small energy-dissipating scales modelled. Promising results have recently been obtained by Hunt and Nixon[50] and Urbin et al[51] for nominally two-dimensional shock wave turbulent boundary layer interactions. The third approach is Engineered Reynolds-averaged Navier-Stokes (ERANS) wherein a CRANS model is modified to improve accuracy for a specific class of flows. ERANS models may include modifications based on knowledge of the flowfield of shock wave turbulent boundary layer interactions (*e.g.*, Coakley and Huang,[52] Panaras[53]) or *ad hoc* modifications for a given configuration (*e.g.*, Bedarev et al[54]).

The objective of this topical group is to assess the capability of DNS, LES and ERANS to predict the aerodynamic and aerothermodynamic properties of configurations with shock wave turbulent boundary layer interactions including strong separation.

Dataset No. 1: 2-D Supersonic Compression Corner

Prepared by

A. Zheltovodov

Description of Experiments

A two dimensional supersonic equilibrium turbulent boundary layer flows past a compression corner of angle α as indicated in Fig. 18. A shock wave is formed by the corner deflection which interacts with the turbulent boundary layer. At sufficiently large corner angle, the boundary layer separates at the corner and shock bifurcates into separation and reattachment compression systems. The test conditions for the selected cases are shown in Table 13. Experimental data of Zheltovodov et al[55–57] includes surface mean pressure, skin friction, adiabatic wall temperature and heat transfer; and boundary layer profiles of mean velocity and temperature and turbulence statistics.
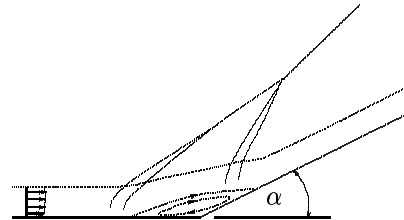

Fig. 18   Compression corner

Table 13   Supersonic Compression Corner

Quantity	Value
M_∞	2.9
Re_δ	7.5×10^4 to 1.5×10^5
α	$8°$ and $25°$

Dataset No. 2: 2-D Expansion-Compression Corner

Prepared by

A. Zheltovodov

Description of Experiments

A two dimensional equilibrium supersonic turbulent boundary layer develops on a flat plate. It expands through an angle α at a corner and subsequently is compressed by an equal angle as illustrated in Fig. 19. The expansion reduces the turbulence kinetic energy and increases the mean kinetic energy in the boundary layer. The turbulence structure within the boundary layer is no longer in equilibrium upon reaching the compression corner. Depending on the compression corner angle, Mach number and Reynolds number, the

---

[i]The term "conventional" implies that there is no problem-specific modification to the general formulation of the particular RANS model.

boundary layer may separate at the compression. Experimental data of Zheltovodov et al[58] is available. The experimental condition for the selected case are shown in Table 14. Additional experimental data is also available.
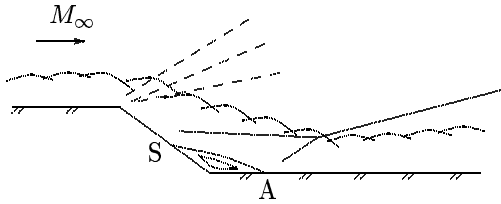

Fig. 19   Expansion compression corner

Table 14   Expansion Compression Corner

Quantity	Value
M_∞	2.9
Re_δ	4.1×10^4 to 1.95×10^5
α	25°

Dataset No. 3: 2-D Shock Impingement

Prepared by

J. Debiéve, M. Eléna, P. Dupont

Description of Experiments

A two-dimensional supersonic equilibrium turbulent boundary layer develops on a flat plate. It is subjected to a shock wave produced by a shock generator (wedge) of angle α placed in the external flow, as indicated in Fig. 20. For sufficiently large angle of yaw of the generator, separation occurs. Although the incident shock is steady, the reflected shock shows significant oscillations. The boundary layer is fully turbulent, but the Reynolds number is rather low, so that the data are appropriate for comparisons with LES computations.
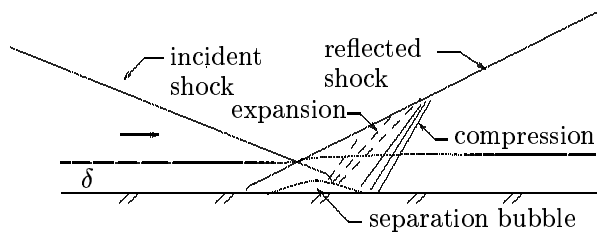

Fig. 20   Shock Impingement

The flow conditions are listed in Table 15. The incoming boundary layer is fully turbulent and develops on a flat plate with nearly adiabatic constant wall temperature. Experimental data are available for generator angles $\alpha = 4°$ and 8°. Experimental data[59–66] include surface mean pressure and mean temperature, boundary layer profiles of mean velocity and temperature, three Reynolds stresses (turbulent friction and two normal stresses), and turbulence statistics on temperature fluctuations. Conditional statistics have been performed to educe the large scale eddies developed

downstream of separation. Statistics of the Strouhal number related to these large scale structures (pdf) have been obtained.

Table 15   Shock impingement

Quantity	Value
M_∞	2.3
Re_δ	5.2×10^4
α	4° and 8°

Dataset No. 4: 3-D Single Fin

Prepared by

D. Knight

Description of Experiments

A two dimensional supersonic equilibrium boundary layer develops on a flat plate. The deflection of the flow by a wedge of angle α (Fig. 21) generates an oblique shock which interacts with the turbulent boundary layer. An extensive set of experiments have been performed for this configuration. Three experiments were selected for CFD validation (Table 16). The experimental data for Case Nos. 1 and 3 are from Zheltovodov et al,[67, 68] and the data for Case No. 2 is from Kim et al.[69] Experimental data include surface pressure, skin friction and surface streamlines.
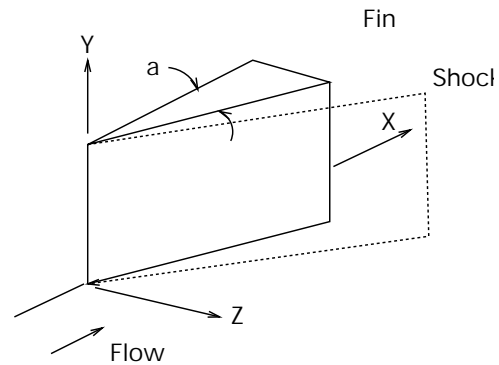

Fig. 21   3-D single fin

Table 16   3-D Single Fin

Case	M_∞	α	Re_δ
1	3.0	15°	1.9×10^5
2	4.0	20°	2.1×10^5
3	4.0	30.6°	1.6×10^5

Dataset No. 5: 3-D Double Fin Interaction No. 1

Prepared by

D. Knight

Description of Experiments

A two-dimensional supersonic equilibrium turbulent boundary layer flows into a rectangular channel formed by two fins of angles α_1 and α_2 attached normal to the flat plate as shown in Fig. 22. Shock waves are

formed by the fin deflections which interact with the turbulent boundary layer on the flat plate. For sufficiently strong shocks, the boundary layer separates into counter-rotating vortices which intersect to form a vortex pair. A complex pattern of shock waves, expansions and slip lines form due to the intersection of the incident shocks. A low total pressure region coincides with the vortex pair. Secondary separation may occur downstream of the intersection of the primary separation lines.
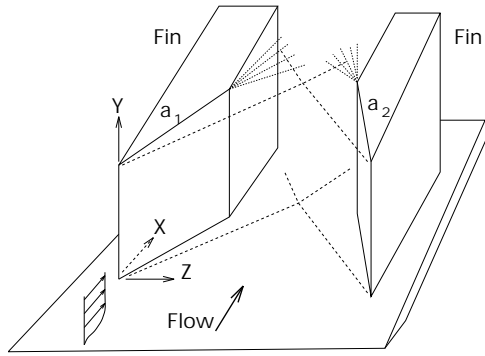

Fig. 22   3-D double fin

The experiments were performed at the Penn State Gas Dynamics Laboratory by Settles *et al.*[70–73] The incoming boundary layer is an equilibrium turbulent boundary layer with an adiabatic or isothermal wall. The flow conditions are indicated in Table 17. Experimental data includes surface pressure, surface flow visualization, Laser Interferometer Skin Friction (LISF) measurements of surface shear stress, flowfield pitot pressure surveys, and Planar Laser Scattering (PLS) images of the flowfield.

Table 17   3-D Double Fin

Case	M_∞	α_1	α_2	Re_δ
1	3.9	9°	9°	2.6×10^5
2	3.9	11°	11°	2.6×10^5
3	3.9	13°	13°	2.6×10^5
4	3.9	15°	15°	2.6×10^5

Dataset No. 6: 3-D Double Fin Interaction No. 2
Prepared by
   A. Zheltovodov, A. Maksimov.

Description of Experiments
   The experiments were performed at the Institute of Theoretical and Applied Mechanics by Zheltovodov *et al.*[74–76] The incoming boundary layer is an equilibrium turbulent boundary layer with an adiabatic or isothermal wall. The flow conditions of the selected experiments are given in Table 18. Experimental data is also available for other configurations. Experimental data includes surface pressure, adiabatic wall temperature, heat transfer and surface flow visualization.

Table 18   3-D Double Fin

Case	M_∞	α_1	α_2	Re_δ
1	4.0	7°	11°	3.0×10^5
2	4.0	15°	15°	3.0×10^5

Dataset No. 7: 3-D Double Fin Interaction No. 3
Prepared by
   A. Zheltovodov, E.Schülein.

Description of Experiments
   The experiments[77–79] were performed at the DLR Institute of Fluid Mechanics, Göttingen, Germany. The configurations are shown in Figs. 23 and 24 where the dimensions are in mm. The incoming boundary layer is an equilibrium turbulent boundary layer with an isothermal wall ($T_w = 290 - 300K$) at Mach 5, $Re_\delta = (1.9 - 2) \times 10^5$, $T_w/T_t = 0.691$. Experimental data is available for fins angles $\beta = 18°$ and $23°$ (Table 19). Experimental data includes surface pressure, surface flow visualization and optical crossing shock wave structure visualization.
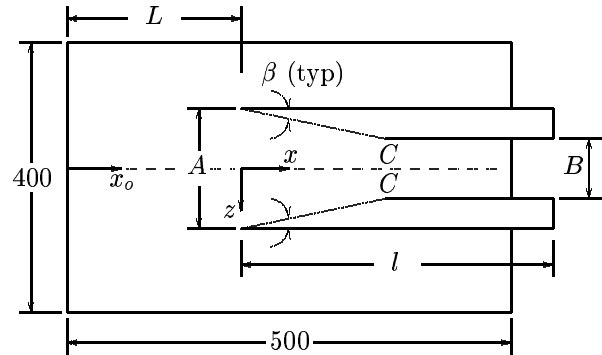

Fig. 23   Short fins ($\beta = 8°, 12°, 18°$)
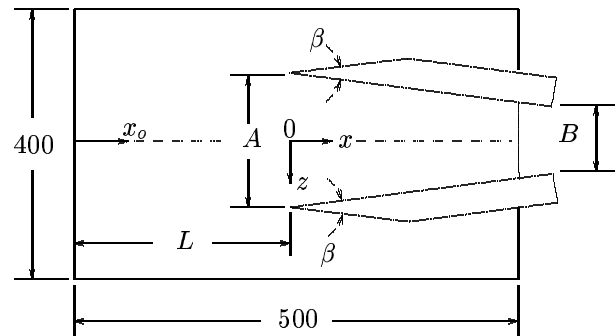
Fig. 24   Long fins ($\beta = 23°$)

Table 19   Double Fin

β	Type	L	A	B	l	
8°	SF	229.5	142.0	100	309	
12°	SF	249.5	161.5	100	280	All
18°	SF	269.0	196.0	100	260	
23°	LF	286.0	307.0	100		

dimensions in mm

Dataset No. 8: Large Cone-Flare

Prepared by

   M. S. Holden

Introduction

   An experimental study[23, 80–82] in which surface and flowfield measurements were made has been conducted to examine the structure of turbulent flow separation over large cone-flare configurations. This study was conducted in Calspan's 96 inch Shock Tunnel at Mach numbers of 11 and 13 with Reynolds numbers up to 100×10^6. The measurements made at the large unit Reynolds number and models employed in this study demonstrated that the attached and separated flows were fully turbulent and a thick boundary layer was developed at the cone/flare junction, which enabled highly resolved measurements in the interaction region. Surface heat transfer and pressure measurements were made in attached and separated flows at the cone-flare junction for 30° and 36° flare angles respectively. Flowfield surveys were made in the separation region with pitot pressure and total temperature rakes. Holographic interferometry and Schlieren photography were used to obtain details of the flowfield structure. This study suggests that, in hypersonic flow, the separation region extends only a very small fraction of the boundary layer thickness and is a highly unsteady process. Only by employing instrumentation with frequency response fast enough to follow the unsteady movement of the separation shock is it possible to determine the fundamental structure of flow separation in turbulent hypersonic flows.

Description of Experiments

   For this study, a large 6° cone with flares of either 30° or 36° attached to its base were employed in the experiment. The cone angle and model length were selected, on the basis of calculations, to achieve the maximum length over which uniform constant-pressure flow could be established within the tunnel. The model configuration is shown in Fig. 25.
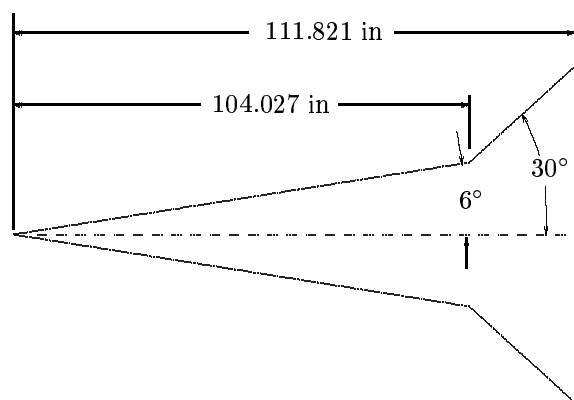

111.821 in

104.027 in

30°

6°

Fig. 25   Large cone-flare

The flowfield is a perfect gas, axisymmetric flowfield, with a well developed turbulent boundary layer. Shock wave-boundary layer interaction and flow separation constitute the principal flowfield physics.

This dataset contains measurements at the largest Mach number and Reynolds number currently available. The experimental data includes surface temperatures, heat transfer and pressure distributions. Additionally, the use of a single-pass Schlieren system with a focal length of 10 feet for flow visualization was used. The freestream conditions are shown in Table 20.

Table 20   Large Cone-Flare

Runs	4,8	6,7
M_i	3.345	3.633
p_0 (psia)	7.216×10^3	1.760×10^4
H_0 (ft^2/sec^2)	1.825×10^7	2.147×10^7
T_0 (°R)	2.717×10^3	3.104×10^3
M	10.96	13.01
U (ft/sec)	5.922×10^3	6.458×10^3
T (°R)	121.4	102.6
p_∞ (psia)	9.172×10^{-2}	7.345×10^{-2}
q_∞ (psia)	7.721	8.712
ρ_∞ (slug/ft^3)	6.340×10^{-5}	6.038×10^{-5}
μ_∞ (slug/ft-sec)	1.021×10^{-7}	8.634×10^{-8}
Re (ft^{-1})	3.680×10^6	4.544×10^6
p_0'(pitot) (psia)	1.431×10^1	1.619×10^1

6. BASE FLOWS WITH AND WITHOUT PLUME INTERACTIONS
TEAM LEADERS: P. BAKKER
P. REIJASSE

Prepared by

   P. G. Bakker and P. Reijasse

Introduction

   For the development of the next generation of reusable launchers and reentry vehicles, one of the critical areas is the proper modelling of the base flow. The low pressures that act on the base region of bodies in supersonic and hypersonic flight can cause significant amounts of drag. Due to separation and reattachment in the baseflow region also the heat loading at the base may be considerable. Futhermore non-axisymmetric effects and unsteadiness can cause severe sideloads on a launch vehicle in the ascent phase. Important parameters influencing the base flow physics are, *e.g.*, boattailing of the afterbody, base bleed, presence of external flow and conditions of the exhausting jet-plume (underexpanded or overexpanded). Three different experimental data sets meeting the WG10 objectives were identified covering most of these effects and (partially) their interactions. Dataset No. 1 (TU-Delft) is a cylindrical afterbody with jet in external flow. Dataset No. 2 (Univ. Illinois) is a cylindrical and boat-tailed afterbody in external flow with no jet. Dataset

No.3 (ONERA) is a boattailed afterbody with jet in external flow. Herrin and Dutton (Dataset No. 2) studied the influence of boattailing in absence of a jet-plume. Their experimental results show that boattailing (without plume) raises the base pressure level and lowers the turbulence levels in the shear layer, so a significant reduction in net afterbody drag results. Dataset Nos. 1 and 3 both deal with external flow and an underexpanded jet-plume. Comparing them we can study the influence of boattailing in presence of a jet-plume (underexpanded).

Dataset No. 1: Base Flow-Plume Interaction in Supersonic External Flow

Prepared by

P. Bakker and W. Bannink

Description of Experiments

The test setup enables the investigation of the flowfield along an axisymmetric body with a single operating exhaust nozzle. The supersonic jet emanating from the centrally protruding exhaust nozzle in the base interacts with the external main flow. Essentially two independant supersonic streams – the external flow and the central jet – interfere at the base region. In the interaction zone a turbulent mixing layer, a recirculating region and a shock system (plume shock, barrel shock, Mach disc) is formed. The model has a conical forebody (semi-apex angle of 11°) with a fair amount of bluntness (nose radius of 7.5 mm) and a cylindrical afterbody (diameter of 50 mm, length of 90 mm). The total length of the model is 186.81 mm. The model is strut-mounted at the lower side and has a free base. From the centre of the base a nozzle protrudes; its outside shape is a circular cylinder. The nozzle itself is conical (total divergence of 15°) having Mach 4 at the exit. The model is positioned in a uniform supersonic free stream at zero incidence. Additional details are presented in Bannink et al.[83,84]

The experimental conditions are shown in Table 21. The boundary layer along the body is tripped at 38 mm from the nose. Experiments are performed at jet pressures (total pressures) ranging from 1.5 MPa to 10 MPa. Due to the unexpected low base pressures it turned out that this pressure range covers only underexpanded jets. Apart from these experiments, experiments without jet are performed as well. Experimental data include mean static surface pressures on afterbody and on the base, Schlieren and shadowgraph pictures of the base flow, and mean Pitot pressures in the base area to capture shock-system and shear layers. New experiments both for $M_\infty = 2$ and $M_\infty = 3$ are underway at jet pressures ranging from 0.3 to 1.2 MPa in order to capture also overexpanded exhaust. Expected experimental data will be similar to those available for the underexpanded case.

Some computational results of two codes based on

Table 21   Base Flow Plume Interaction

M_∞	Re_L	p_{t_∞}	T_{t_∞}
2	5.16×10^6	0.206 MPa	285 K
3	8.70×10^6	0.575 MPa	285 K

the RANS equations are available. Houtman (TU-Delft) has performed numerical simulations using a code based on a cell centered finite volume discretization of the Euler- and the Navier-Stokes equations. The code is equipped with the one-equation Spalart-Almaras turbulence model. Structured multiblock grids are used. Van der Weide (von Karman Institute) has used a code based on a multidimensinal upwinding method on unstructured grids. Various turbulence models (*e.g.*, Spalart-Almaras, BSL and SST) are used. The computational results only show good agreement with experiments in the not viscous dominated parts of the flowfield. The prediction of the base flow however, appears a tough problem which requires extremely fine grids, especially for the two-equation models. The calculated base pressures are still significantly lower than those found in the experiments.

Dataset No. 2: Supersonic Axisymmetric Base Flows Including Boattail Effects

Prepared by

P. Bakker and W. Bannink

Description of Experiments

The configuration enables detailed non-intrusive measurements on the entire near-wake flowfield structure behind a cylindrical and a boattailed afterbody immersed in a supersonic flow. The near-wake is characterized by the occurrence of separating shear layers reattaching downstream, and enclosing a recirculation region. The base model is mounted on a central sting which supports the model from upstream. The cylindrical part of the afterbody used in the experiments is 63.5 mm diameter.

Table 22   Base Flow

M_∞	Re/m	p_{t_∞}	T_{t_∞}
2.46	5.2×10^7	0.515 MPa	294 K

Experiments were performed at the University of Illinois Urbana-Champaign by Dutton et al.[85–88] The flow conditions are shown in Table 22. Oilstreak visualization and micrometer measurements were performed to attain an axisymmetric flow. Experimental data include Schlieren and shadowgraph pictures of the near-wake flow, mean static pressures at several locations on the base and on the afterbody surfaces, and two-component LDV measurements in the boundary layer approaching the base corner and in the near-wake region. From the detailed quantitative data obtained in the near-wake, specifically afterbody and base pressure distributions, mean velocities, turbulence intensities and Reynolds shear stresses have been obtained.

Dataset No. 3: Plume-Induced Flow Separation on a Jet-On Axisymmetric Boattailed Afterbody

Prepared by

P. Reijasse, B. Corbel

Introduction

These experiments[89] have been performed under contract of the French Ministry of Defense to constitute a Navier-Stokes validation test case regarding the pluming phenomena of an underexpanded propulsive jet which induces the external flow separation on a axisymmetric afterbody boattail. The tests have been carried out in the S8Ch continuous atmospheric subsonic/supersonic research windtunnel in the Fundamental and Experimental Aerodynamics Department of ONERA, headed by Prof. J. Délery.

Description of Experiments

The S8Ch wind tunnel was equipped with two planar converging-diverging half-nozzles. The test section is 0.12 m x 0.12 m. The axisymmetric model is supported by an upstream central sting fixed in the settling chamber. A sketch of the model is shown in Fig. 26. The external diameter D of the model is 30 mm. The aft part of the model is a 9B05 boattail having a length of 31.5 mm. The model is equipped of a 10B0 conical nozzle having an exit diameter of 14.9 mm. The origin of the coordinate system is located in the exit plane of the model nozzle on the symmetry axis. The mesh coordinates are nondimensionalized by the model diameter D.
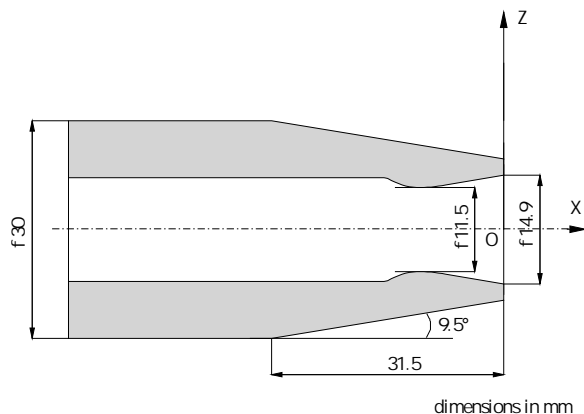

dimensions in mm

Fig. 26   Jet-on boattailed afterbody

The afterbody region of the model is subject to complex interactions due to flow confluence between the propulsive jet and the outer flow. After the upstream external flow crosses the expansion waves centered on the boattail origin, it meets an interaction shock located at the middle of the boattail. This shock wave / boundary layer interaction, resulting in the separation of the external boundary layer, is induced by the pluming of the jet, with the underexpanded jet behaving as a "fluid ramp" facing to the incoming external flow. The interaction shock coalesces with the confluence shock crossing the external flow. Downstream of the nozzle exit, the jet is accelerated when it crosses the expansion waves centered on the nozzle lip. The thin jet shear layer rapidly thickens when it reaches the confluence region. Then the confluence process starts the development of a wake which ensures the mutual adaptation of the flows. The jet internal shock – or barrel shock – which results from the Mach lines focusing process, reflects on the symmetry axis in a singular way with the formation of a Mach disk structure.

The experimental database includes wall pressure on the afterbody boattail and on the base, spark and continuous Schlieren photographs, and 2000 measurement points by the two-component laser velocimeter technique giving the mean streamwise and radial components of the velocity, the streamwise and radial turbulence intensities, the turbulent shear stress and an approximation of the turbulence kinetic energy.

Freestream conditions are given in Table 23. The unit Reynolds number is equal to 12.24×10^6 m^{-1}.

Table 23   Jet-on Boattailed Afterbody

Flow parameter	External Flow	Jet Flow
Specific heat ratio	1.4	1.4
p_t (bar)	0.975	7.75
T_t (K)	298	298
M	1.94	1.75

Acknowledgments

References

[1]Saric, W., Reshotko, E., and Arnal, D., "Hypersonic Laminar-Turbulent Transition", in AGARD AR-319, Volume II, Dec. 1998.

[2]Schneider, S., "Flight Data for Boundary-Layer Transition at Hypersonic and Supersonic Speeds", *J. Spacecraft and Rockets*, Vol. 36, No. 1, pp. 8–20, January 1999.

[3]Schneider, S., "Effects of High-Speed Tunnel Noise on Laminar-Turbulent Transition", *J. of Spacecraft and Rockets*, Vol. 38, No. 3, pp. 323–333, May–June 2001.

[4]Reshotko, E., "A Program for Transition Research", *AIAA Journal*, Vol. 13, No. 3, March 1975, pp. 261–265.

[5]Schneider, S., "Hypersonic Laminar Instability on Round Cones Near Zero Angle of Attack", AIAA Paper No. 2001-0206, January 2001.

[6]Hornung, H., and Lemieux, P., "Shock Layer Instability Near the Newtonian Limit of Hypervelocity Flows", *Physics of Fluids*, Vol. 13, No. 8, August 2001, pp. 2394–2402.

[7]Stetson, K., Thompson, E., Donaldson, J., and Siler, L., "Laminar Boundary Layer Stability Experiments on a Cone at Mach 8, Part 1: Sharp Cone," AIAA Paper No. 83-1761, July 1983.

[8]Stetson, K. and Kimmel, R., "On Hypersonic Boundary-Layer Stability," AIAA Paper No. 92-0737, January 1992.

[9]Stetson, K.F., Thompson, E.R., Donaldson, J.C., and Siler, L.G., "Laminar Boundary Layer Stability Experiments on a Cone at Mach 8, Part 2: Blunt Cone," AIAA Paper No. 84-0006, January 1984.

[10]Donaldson, J. and Coulter, S., "A Review of Free-Stream Flow Fluctuation and Steady-State Flow Quality Measurements in the AEDC/VKF Supersonic Tunnel A and Hypersonic Tunnel B," AIAA Paper No. 96-6137, April 1995.

[11]Herbert, T. and Esfahanian, V., "Stability of Hypersonic Flow over a Blunt Body," Paper 28 in AGARD CP-514, *Theoretical and Experimental Methods in Hypersonic Flows*, May 1992.

[12]Kufner, E. and U. Dallman, "Entropy- and Boundary Layer Instability of Hypersonic Cone Flows – Effects of Mean Flow Variations," in *Laminar-Turbulent Transition - Proceedings of the IUTAM Symposium*, Sendai, Japan, Springer-Verlag, Berlin, 1995, pp. 197–204.

[13]Kimmel, R., "Hypersonic Boundary Layer Stability Measurements Using Uncalibrated Hot Wires", AIAA Paper No. 2001-0275, January 2001.

[14]Lachowicz, J., Chokani, N., and Wilkinson, S., "Boundary-Layer Stability Measurements in a Hypersonic Quiet Tunnel," *AIAA Journal*, Vol. 34, No. 12, Dec. 1996, pp. 2496–2500.

[15]Lachowicz, J., Chokani, N., and Wilkinson, S., "Hypersonic Boundary Layer Stability over a Flared Cone in a Quiet Tunnel," AIAA Paper No. 96-0782, January 1996.

[16]Lachowicz, J., and Chokani, N., "Hypersonic Boundary Layer Stability Experiments in a Quiet Wind Tunnel with Bluntness Effects," NASA CR-198272, January 1996.

[17]Blanchard, A., Lachowicz, J., and Wilkinson, S., "NASA Langley Mach 6 Quiet Wind-Tunnel Performance," *AIAA Journal*, Vol. 35, No. 1, January 1997, pp. 23–28.

[18]Riemann, C., Chokani, N., and Sarma, G., "Calibrated Measurements Using a CVA-Operated Hot-Wire in a Hypersonic Laminar Boundary Layer", AIAA Paper No. 2002-0152, January 2002.

[19]Balakumar, P. and Malik, M., "Effect of Adverse Pressure Gradient and Wall Cooling on Instability of Hypersonic Boundary Layers," High Technology Corporation Report HTC-9404, March 1994.

[20]Pruett, C. and Chang, C.-L., "Direct Numerical Simulation of Hypersonic Boundary-Layer Flow on a Flared Cone," *Theoretical and Computational Fluid Dynamics*, Vol. 11, No. 1, March 1998, pp. 49–67.

[21]Holden, M., "Shock Interaction Phenomena in Hypersonic Flows", AIAA Paper No. 98-2751, June 1998.

[22]Holden, M., "Experimental Database for CFD Validation of Hypersonic Laminar Separated Flows in the Absence of and with Flowfield Chemistry", Calspan - University of Buffalo Research Center, February 1999.

[23]Holden, M., "Database of Aerothermal Measurements in Hypersonic Flow for CFD Validation", CUBDAT Version 2.2 CD-ROM, Calspan - University at Buffalo Research Center, 1999.

[24]Holden, M.,"Shock Interaction in Hypersonic Flows", AIAA Paper No. 98-2751, June 1998.

[25]Holden, M., "Experimental Database for CFD Validation for RTO Working Group 10", Calspan - University of Buffalo Research Center, June 1999.

[26]Chanetz, B., Bur, R., Pot, T., Pigache, D., Gorchakova, N., Moss, J., and Schulte, D., "Study of the Shock Wave/Boundary Layer Interactions in Low Density Hypersonic Flow: Comparisons between Flowfield Measurements and Numerical Results," Proceeding of the Conference on the 21st Rarefied Gas Dynamics, Marseille, France, July 26-31, 1998.

[27]Chanetz, B., Benay, R., Bousquet, J. M., Bur, R., Oswald, J., Pot, T., Grasso F., and Moss, J., "Experimental and Numerical Study of the Laminar Separation in the Hypersonic Flow," *Aerospace Science and Technology*, No. 3, 205–218, 1998.

[28]Chanetz, B., Benay, R., Bousquet, J., M., Bur, R., Oswald, J., Pot, T., Grasso, F., and Moss, J., "Study of the laminar Shock Wave-Boundary Layer Interaction in Hypersonic Flow : Experimental and Numerical Aspects", First Europe-US High Speed Flow Field Database Workshop, CIRA, Naples, Italy, November 12–14, 1997.

[29]Holden, M., and Wadhams, T., "Code Validation Study of Laminar Shock / Boundary Layer and Shock / Shock Interactions in Hypersonic Flow. Part A: Experimental Measurements", AIAA Paper No. 2001-1031 (Part A).

[30]Wright, M., Sinha, K., and Candler, G., "The Effect of Turbulence on Double-Cone Shock Interactions", AIAA Paper No. No. 99-0146, January 1999.

[31]Pot, T., Chanetz, B., Lefebvre M., and Bouchardy, P., "Fundamental Study of Shock-Shock Interference in Low Density Flow : Flowfield Measurements by DLCARS", Proceeding of the Conference on the 21st Rarefied Gas Dynamics, Marseille, France, July 26–31, 1998. ONERA TP No. 1998-140, Rarefied Gas Dynamics, Brun, R., Campargue, R., Gatignol, R., and Lengrand, J.-C. (Eds.), CEPADUES EDITIONS, Toulouse, France, pp. 545–552 (Vol. 2).

[32]Moss, J., Pot, T., Chanetz, B., and Lefebvre, M., "DSMC Simulation of Shock / Shock Interactions: Emphasis on Type IV Interactions", *Proceedings of the 22nd International Symposium on Shock Waves*, London, July 18-23, 1999. Also, ONERA TP No. 1999-107.

[33]Délery, J., and Chanetz, B., "Experimental Aspects of Code Verification / Validation: Application to Internal Aerodynamics", VKI Lecture Series on Verification and Validation of Computational Fluid Dynamics, June 5-8, 2000. Also, ONERA TP No. 2000-155.

[34]Reijasse, P., Bur, R., and Chanetz, B., "The French Program PREPHA: Experimental Analysis of Aerodynamic Interactions Occuring on a Hypersonic Spacecraft", *Journal of Spacecraft and Rockets*, Vol. 38, No. 2, 2001, pp. 129–135.

[35]Holden, M., Sweet, S., Kolly, J., Smolinski, G., "A Review of the Aerothermal Characteristics of Laminar, Transitional and Turbulent Shock/Shock Interaction Regions in Hypersonic Flows," AIAA Paper 98-0899, January 1998.

[36]Holden, M., Kolly, J., Smolinski, G., Sweet, S., Moselle, J., "Studies of Shock/Shock Interaction in Regions of Laminar, Transitional and Turbulent Hypersonic Flows," NASA Report NAG-1-1339, February 1998.

[37]Ivanov, M., Gimelshein, S., Beylich, A., "Hysteresis Effect in Stationary Reflection of Shock Waves", *Physics of Fluids*, Vol. 7, No. 4, 1995, pp. 685–687.

[38]Ivanov, M., Khotyanovsky, D., Kudryavtsev, A., and Nikiforov, S., "Experimental Study of 3-D Shock Wave Configurations During ↔ MR Transition", *23rd International Symposium on Shock Waves*, 2001.

[39]Ivanov, M., Klemenkov, G., Kudryavtsev, A., Nikiforov, S., Pavlov, A., Fomin, V., Kharitonov, A., and Khotyanovsky, D., "Experimental and Numerical Study of the Transition Between Regular and Mach Reflection of Shock Waves in Steady Flows", *Proceedings of the 21st International Symposium on*

Shock Waves, Great Keppel, Australia, Vol. 2, 1997, pp. 819–824.

[40]Ivanov, M., Markelov, G., Kudryavtsev, A., and Gimelshein, S., "Numerical Analysis of Shock Wave Reflection Transition in Steady Flows", *AIAA Journal*, Vol. 36, No. 11, 1998, pp. 2079–2086.

[41]Ivanov, M., Klemenkov, G., Kudryavtsev, A., Nikiforov, S., Pavlov, A., Kharitonov, A., and Fomin, V., "Wind Tunnel Experiments on Shock Wave Reflection Transition and Hysteresis", *Proceedings of the 22nd International Symposium on Shock Waves*, 1999, London, UK.

[42]Ivanov, M., Klemenkov, G., Kudryavtsev, A., Nikiforov, S., Pavlov, A., Fomin, V., Kharitonov, A., and Khotyanovsky, D., "Experimental and Numerical Study of the Transition Between Regular and Mach Reflection of Shock Waves in Steady Flows", *Proceedings of the 21st International Symposium on Shock Waves*, Great Keppel, Australia, Vol. 2, 1997, pp. 819–824.

[43]Ivanov, M., Gimelshein, S., Kudryavtsev, A., Markelov, G., Khotyanovsky, D., "Numerical Simulation of Three-Dimensional Regular and Mach Reflections of Shock-Waves in Steady Flows", *Proceedings of the 4th European Computational Fluid Dynamics Conference*, Athens, Greece, Vol. 1, Part 2, 1998, pp. 869–874.

[44]Kudryavtsev, A., Khotyanovsky, D., Markelov, G., Ivanov, M., "Numerical Simulation of Reflection of Shock Waves Generated by Finite-Width Wedge", *Proceedings of the 22nd International Symposium on Shock Waves*, 1999, London, UK.

[45]Knight, D., "Numerical Simulation of 3-D Shock Wave Turbulent Boundary Layer Interactions", AGARD - VKI Special Course on Shock- Wave Boundary-Layer Interactions in Supersonic and Hypersonic Flows, G. Degrez (editor), von Karman Institute for Fluid Dynamics, AGARD R-792, pp. 3-1 to 3-32.

[46]Dolling, D., "Considerations in the Comparison of Experimental Data with Simulations – Consistency of Math Models and Flow Physics", AIAA Paper No. 96-2030, June 1996.

[47]Zheltovodov, A., "Shock Waves / Turbulent Boundary Layer Interactions– Fundamental Studies and Applications", AIAA Paper 96-1977, June 1996.

[48]Knight, D., and Degrez, G., "Shock Wave Boundary Layer Interactions in High Mach Number Flows: A Critical Survey of Current Numerical Prediction Capabilities", AGARD Advisory Report AR–319, Vol. II.

[49]Zheltovodov, A., Borisov, A., Knight, D., Horstman, C., and Settles, G., "The Possibilities of Numerical Simulation of Shock Waves Boundary Layer Interaction in Supersonic and Hypersonic Flows", *International Conference on the Methods of Aerophysical Research*, Russian Academy of Sciences, Siberian Division, pp. 164–170, 1992.

[50]Hunt, D., and Nixon, D., "A Very Large Eddy Simulation of an Unsteady Shock Wave Turbulent Boundary Layer Interaction", AIAA Paper 95-2212, June 1995.

[51]Urbin, G., Knight, D., and Zheltovodov, A., "Compressible Large Eddy Simulation Using Unstructured Grids: Supersonic Turbulent Boundary Layer and Compression Corner", AIAA Paper No. 99-0427, January 1999.

[52]Coakley, T., and Huang, P., "Modeling for Compressible High Speed Flows", Tenth National Aerospace Plane Technology Symposium, Paper No. 210.

[53]Panaras, A., "The Effect of the Structure of Swept Shock Wave Turbulent Boundary Layer Interactions on Turbulence Modelling", *Journal of Fluid Mechanics*, Vol. 338, pp. 203–230.

[54]Bedarev, I., Zheltovodov, A., and Fedorova, N., "Supersonic Turbulent Separated Flows Numerical Model Verification", *International Conference on the Methods of Aerophysical Research*, Russian Academy of Sciences, Siberian Division, Part I, pp. 30–35, 1998.

[55]Zheltovodov, A., and Yakovlev, V., "Stages of Development, Flowfield Structure and Turbulence Characteristics of Compressible Separated Flows in the Vicinity of 2-D Obstacles", Preprint No. 27-86, Institute of Theoretical and Applied Mechanics, USSR Academy of Sciences, Novosibirsk, 1986, 56 pp. (in Russian).

[56]Zheltovodov, A., Schülein, E., Yakovlev, V., "Development of Turbulent Boundary Layer under Conditions of Mixed Interaction with Shock and Expansion Waves", Preprint No. 28-83, Institute of Theoretical and Applied Mechanics, USSR Academy of Sciences, Novosibirsk 1983, 51 p. (In Russian).

[57]Zheltovodov, A., Trofimov, V., Schülein, E., and Yakovlev, V., "An Experimental Documentation of Supersonic Turbulent Flows in the Vicinity of Forward- and Backward-Facing Ramps", Report No. 2030, Institute of Theoretical and Applied Mechanics, USSR Academy of Sciences, 1990.

[58]Zheltovodov, A., Schülein, E., and Horstman, C., "Development of Separation in the Region Where a Shock Interacts with a Turbulent Boundary Layer Perturbed by Rarefaction Waves", *Journal of Applied Mechanics and Technical Physics*, Vol. 34, No. 3, May-June 1993, pp. 346–354.

[59]N. Audiffren, "Turbulence d'une couche limite soumise à une variation de densité due à une onde de choc ou à un chauffage pariétal", Univ. Aix-Marseille II, Marseille, France, March 1993.

[60]N. Audiffren, J. Deleuze, M. Eléna, "Remarques sur le comportement des tensions de Reynolds dans une interaction onde de choc couche limite turbulente", C. R. Acad. Sc. Paris, t. 321 , Série IIb, 1995.

[61]J. Deleuze, "Structure d'une couche limite turbulente soumise à une onde de choc incidente", Thèse de Doctorat, Université d' Aix-Marseille II, Marseille, France, Sept. 1995.

[62]M. Eléna, J.F. Debiève, J. Deleuze, H. Laurent, "Interaction entre une couche limite turbulente et une onde de choc incidente", Final Report, Contract DRET 93/2539A, Avril 1995.

[63]J. Deleuze, M. Eléna, "Quelques caractéristiques de la turbulence en aval d'une interaction onde de choc / couche limite", Proceedings of the 12th Congrès François de Mécanique, 4- 8th September 1995, Strasbourg, France.

[64]J. Deleuze, M. Eléna, "Some Turbulence Characteristics Downstream of a Shock Wave Boundary Layer Interaction", Advances in Turbulence VI, S. Gavrilakis, L. Machiels, P. Monkewitz Ed., Kluwer Academic Publishers, 1996, pp. 433-436.

[65]H. Laurent, "Turbulence d'une interaction onde de choc/couche limite sur une paroi plane adiabatique ou chauffée.", Université d' Aix-Marseille II, Marseille, France, May 1996.

[66]P. Dupont, J.F. Debiève, Etude et réalisation d'une base de données en vue de la validation de calculs de simulation des grandes échelles en écoulement comprenant des chocs", Final Report Contract DGA/DSA-SpAe 95 006, BC38, Poste 5.

[67]Zheltovodov, A., "Regimes and Properties of Three-Dimensional Separation Flows Initiated by Skewed Compression Shocks", *Journal of Applied Mechanics and Technical Physics*, Vol. 23, No. 3, May-June 1982, pp. 413–418.

[68]Zheltovodov, A., and Schülein, E., "Three Dimensional Interaction of Swept Shock Waves with Turbulent Boundary Layer in Corner Configurations", Institute of Theoretical and Applied Mechanics Preprint 34-86, USSR Academy of Sciences, Novosibirsk, 1986, 49 pp. (in Russian).

[69]Kim, K., Lee, Y., Alvi, F., Settles, G., and Horstman, C., "Skin Friction Measurements and Computational Comparison of Swept Shock Boundary Layer Interactions", *AIAA Journal*, Vol. 29, No. 10, 1991, pp 1643–1650.

[70]Garrison, T., and Settles, G., "Flowfield Visualization of Crossing Shock Wave Boundary Layer Interactions", AIAA Paper No. 92-0750, 1992.

[71]Garrison, T., and Settles, G., "Interaction Strength and Model Geometry Effects on the Structure of Crossing Shock Wave Turbulent Boundary Layer Interactions", AIAA Paper No. 93-0780, 1993.

[72]Garrison, T., and Settles, G., "Laser Interferometer Skin Friction Measurements of Crossing Shock Wave Turbulent Boundary Layer Interactions", AIAA Paper No. 93-3072, 1993.

[73]Garrison, T., Settles, G., Narayanswami, N., Knight, D., and Horstman, C., "Flowfield Surveys and Computations of a Crossing Shock Wave Boundary Layer Interaction", *AIAA Journal*, Vol. 34, pp. 50–56, 1996.

[74]Zheltovodov, A., and Maksimov, A., "Symmetric and Asymmetric Crossing Shock Waves Turbulent Boundary Layer Interactions", Final Report, EOARD Contract F61708-97-W0136, Institute of Theoretical and Applied Mechanics, Novosibirsk, Russia, 1998.

[75]Zheltovodov, A., Maksimov, A., Shevchenko, A., "Topology of Three-Dimensional Separation Under the Conditions of Symmetrical Interaction of Crossing Shocks and Expansion Waves with Turbulent Boundary Layer", *Thermophysics and Aeromechanics*, Vol. 5, No. 3, pp. 293–312, 1998.

[76]Zheltovodov, A., Maksimov, A., Shevchenko, A., and Knight, D. "Topology of Three Dimensional Separation Under the Conditions of Asymmetrical Interaction of Crossing Shocks and Expansion Waves with Turbulent Boundary Layer", *Thermophysics and Aeromechanics*, Vol. 5, No. 4, pp. 483–503, 1998.

[77]Schuelein, E. and Zheltovodov A., "Development of Experimental Methods for the Hypersonic Flows Studies in Ludwieg Tube", *International Conference on the Methods of Aerophysical Research: Proceedings Part 1*, Novosibirsk, Russia 29 June – 3 July 1998. Novosibirsk, 1998, pp. 191–199.

[78]Zheltovodov, A. and Maksimov A., "Hypersonic Crossing-Shock-Waves/Turbulent Boundary Layer Interactions", Final Report, EOARD Contract F61775-98-WE091, Institute of Theoretical and Applied Mechanics, Novosibirsk, Russia, 1999, 78 pg.

[79]Zheltovodov, A., Maksimov, A., Gaitonde, D., Schmisseur, J., and Schuelein, E., "Verification of Crossing-Shock-Wave Boundary Layer Interaction Computations with $k-\epsilon$ Turbulence Model", *International Conference on the Methods of Aerophysical Research: Proceedings*, Novosibirsk, 2000.

[80]Holden, M., "Studies of Mean and Unsteady Structure of Turbulent Boundary Layer Separation in Hypersonic Flow", AIAA Paper No. 91-1778, June 1991.

[81]Holden, M., "Shock Wave-Turbulent Boundary Layer Interaction in Hypersonic Flow", AIAA Paper No. 77-45, January 1977.

[82]Holden, M.,"Shock Wave-Turbulent Boundary Layer Interaction in Hypersonic Flow", AIAA Paper No. 72-74, January 1972.

[83]Bannink, W., Bakker, P. and Houtman, E., "FESTIP Aerothermodynamics: Experimental Investigation of Base Flow and External Plume Interaction", Memorandum M-775, Aerospace Engineering, Delft University of Technology, 24 pg, 1997.

[84]Bannink, W., Houtman, E. and Bakker, P., "Base Flow/Underexpanded Exhaust Plume Interaction in a Supersonic External Flow", AIAA Paper No. 98-1598, AIAA 8th International Space Planes and Hypersonic Systems and Technologies Conference, April 1998, 11 pg., 1998.

[85]Herrin, J. L., and Dutton, J., "Supersonic Base Flow Experiments in the Near Wake of a Cylindrical Afterbody", *AIAA Journal*, Vol. 32, No. 1, January 1994, pp. 77–83, 1994.

[86]Herrin, J. and Dutton, J., "An Experimental Investigation of Supersonic Axisymmetric Base Flow Including the Effects of Afterbody Boattailing", UILU ENG93-4018, University of Illinois, 1993.

[87]Herrin, J. and Dutton, J., "Effects of Afterbody Boattailing on the Near-Wake of Axisymmetric Bodies in Supersonic Flow", AIAA Paper No. 94-0029, January 1994.

[88]Dutton, J. *et al*, "Recent Progress on High Speed Separated Base Flows", AIAA Paper No. 95-0472, January 1995.

[89]Reijasse, P., Corbel, C., "Décollement de l'Ecoulement externe induit par l'éclatement du jet propulsif sur un rétreint d'arrière-corps de missile (External Flow Separation Induced by the Jet Pluming on a Missile Afterbody Boattail)," 34th Applied Aerodynamics Conference of the French Association for Aeronautics and Astronautics, Marseille, France, March 23-25, 1998.